PB-239 690

DEVELOPMENT OF AIR PARTICULATE MONITORING SYSTEMS

F. S. Goulding, et al

California University

Prepared for:

National Environmental Research Center

May 1974

DISTRIBUTED BY:

NTIS

National Technical Information Service
U. S. DEPARTMENT OF COMMERCE

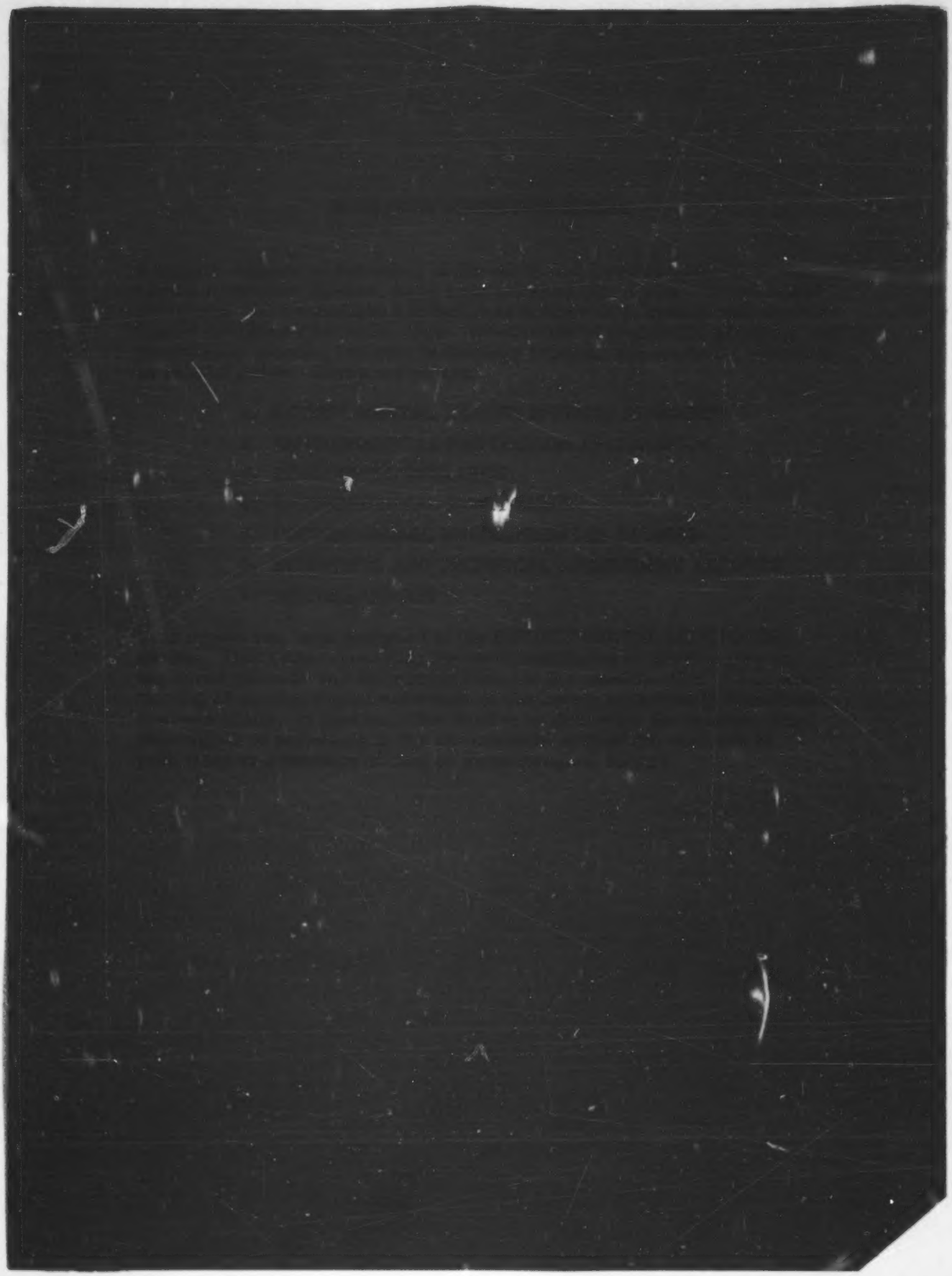

TECHNICAL REPORT DATA
(Please read Instructions on the reverse before completing)

1. REPORT NO. EPA-650/4-74-030	2. PB 239 690
4. TITLE AND SUBTITLE: Development of Air Particulate Monitoring Systems	5. REPORT DATE: May 1974
	6. PERFORMING ORGANIZATION CODE
7. AUTHOR(S): F. S. Goulding and J. M. Jaklevic	8. PERFORMING ORGANIZATION REPORT NO.
9. PERFORMING ORGANIZATION NAME AND ADDRESS: Lawrence Berkeley Laboratory, University of California, Berkeley, California 94720	10. PROGRAM ELEMENT NO. 1A1103
	11. CONTRACT/GRANT NO. IAG-04-0377
12. SPONSORING AGENCY NAME AND ADDRESS: Environmental Protection Agency, National Environmental Research Center, Research Triangle Park, N. C. 27711	13. TYPE OF REPORT AND PERIOD COVERED: Final Jan. 1973 to Jan. 1974
	14. SPONSORING AGENCY CODE

15. SUPPLEMENTARY NOTES

16. ABSTRACT

Progress is described for the first year of a two year effort to fabricate a high-speed aerosol analysis system. Twelve automated dichotomous sampling stations which collect particles in the 0 to 2 and 2 to 20-μm diameter ranges will be built. An evaluation of a prototype virtual impactor for aerodynamically separating particles into two size ranges is given. Design improvements for minimizing losses are described. Design parameters have been determined for a high-speed energy dispersive X-ray fluorescence spectrometer capable of analysis of elements with atomic numbers above 13. A prototype beta gauge for total mass determination has been tested, and a detection limit of 10 $\mu g/cm^2$ has been measured. For the purpose of sample identification, a system is described by which the X-ray spectrometer and the beta gauge will be able to identify a digital code marked on each filter.

Reproduced by
NATIONAL TECHNICAL
INFORMATION SERVICE
US Department of Commerce
Springfield, VA. 22151

17. KEY WORDS AND DOCUMENT ANALYSIS

a. DESCRIPTORS	b. IDENTIFIERS/OPEN ENDED TERMS	c. COSATI Field/Group
Airborne Particulate Monitor Aerosol Size Fractionation X-ray Fluorescence X-ray tubes Trace Element Analysis Beta Gauge Mass Monitor		

PRICES SUBJECT TO CHANGE

18. DISTRIBUTION STATEMENT: Release Unlimited	19. SECURITY CLASS *(This Report)*: UNCLASSIFIED	21. NO. OF PAGES: 67
	20. SECURITY CLASS *(This page)*: UNCLASSIFIED	22. PRICE: 4.25 - 2.25

EPA Form 2220-1 (9-73)

U.S. GOVERNMENT PRINTING OFFICE: 1974 - 640-878/638 - Region 4

EPA-650/4-74-030

DEVELOPMENT OF AIR PARTICULATE MONITORING SYSTEMS

by

F. S. Goulding and J. M. Jaklevic

Lawrence Berkeley Laboratory
Berkeley, California 94720

Interagency Agreement No. EPA-IAG-D4-0377
ROAP No. 56AAI
Program Element No. 1A1103

EPA Project Officer: T. G. Dzubay

Chemistry and Physics Laboratory
National Environmental Research Center
Research Triangle Park, North Carolina 27711

Prepared for

OFFICE OF RESEARCH AND DEVELOPMENT
U.S. ENVIRONMENTAL PROTECTION AGENCY
WASHINGTON, D.C. 20460

July 1974

EPA REVIEW NOTICE

This report has been reviewed by the National Environmental Research Center - Research Triangle Park, Office of Research and Development, EPA, and approved for publication. Approval does not signify that the contents necessarily reflect the views and policies of the Environmental Protection Agency, nor does mention of trade names or commercial products constitute endorsement or recommendation for use.

This document is available to the public for sale through the National Technical Information Service, Springfield, Virginia 22161.

TABLE OF CONTENTS

I. INTRODUCTION 1

II. IMPROVEMENTS IN COMPUTER PROCESSING 3

III. PARTICLE SIZING 3

A. Objectives 3

B. Approach 5

C. Progress and Results 6

1. Description of ERC unit 7

2. Loss measurement method 7

3. Experimental procedure in loss measurement . . . 8

4. Results on ERC impactor 10

5. Summary of evaluation of ERC unit 14

6. Work on new dichotomous sampler 15

IV. PULSED X-RAY TUBE 18

A. Objectives 18

B. Tube Design 20

1. Cathode-grid assembly 20

2. Electron optics 21

3. Switching characteristics 23

C. Electronic Design 24

1. Grid pulse circuit 24

2. X-ray control loop 25

D. Mechanical Design 27

E. Results 28

F. Conclusion 32

V. DIGITAL FILTER MARKING 33

VI. TOTAL PARTICULATE MEASUREMENT 34

References and Footnotes 36

Figure Captions 37

Appendix A 58

I. INTRODUCTION

This report describes progress achieved during the calender year 1973 on work carried out under an Interagency Agreement between the Environmental Protection Agency and the Atomic Energy Commission. The program concerns several aspects of air particulate analysis using energy-dispersive X-ray fluorescence elemental analysis techniques. The 1973 project is a direct continuation of the 1972 program* during which a particulate collection and analysis system was developed and delivered to the EPA laboratories at Research Triangle Park, North Carolina. This system provides for automatic sample collection, and also for automatic elemental analysis using an X-ray fluorescence analyzer under the control of a Texas Instrument 960A computer. The 1973 program has been directed toward a number of improvements and additions to the monitoring system with particular emphasis on developing the concepts, hardware and computer programs required for the large-scale St. Louis RAPS program to be carried out toward the end of 1974. Aspects requiring particular attention included:

i) Improvements in the X-ray spectral analysis program to facilitate its use and to improve the accuracy of results. This has required continuous contact with EPA personnel using the system at Research Triangle Park, and the changes made reflect experience in use of this system.

ii) The importance of separating small particles from large ones, both for medical reasons and as an aid in pinpointing origins of various elements, has led to the requirement for collecting two parallel samples

per collecting station, each representing a different size range (less and greater than 2 micron diameter). To satisfy this requirement a dichotomous sampler has been developed which deposits particles from the two size ranges on separate filters which may then be analyzed by the X-ray system.

iii) In order to speed up the X-ray analysis process, work has been carried out on a pulsed X-ray system[1] which should reduce the analysis time by approximately a factor of four compared with the earlier EPA system.

iv) The handling of very large numbers of samples will be facilitated by digital marking of all filters prior to use and subsequently reading of this marking by the computer during elemental analysis. Various methods of marking have been studied and one has been chosen for use in the St. Louis RAPS program.

v) Since total particulate mass measurements are required in the St. Louis RAPS program, a strategy has been developed for using a beta-gauging technique on the same filters as used for elemental analysis. The digital marking facilitates keeping records of the filter mass before and after exposure.

The following detailed discussion will be broken down into these five sections.

II. IMPROVEMENTS IN COMPUTER PROCESSING

A number of changes in the hardware and software associated with the TI-960 computer were implemented during the contract period. These improvements were concerned both with expanding the data handling capabilities and increasing the convenience and reliability of the existing system. These changes are detailed in Appendix A.

III. PARTICLE SIZING

A. Objectives

Interest in size separation of atmosphere particles results from the desire to obtain size vs. elemental concentration correlations as part of a complete aerosol monitoring and characterization program. The size distribution of suspended particulates and the related elemental distributions are important both in determining the origin and history of the atmospheric aerosol, and in the assessment of respiratory health effects.

Most existing particle size separators depend upon the impaction of particles on surfaces placed in a rapidly moving air stream. The change in direction as the air stream is deflected by the surface causes particles above a certain critical size to be impacted onto it. By cascading a number of these impactor stages with successively smaller critical size cut-offs, a series of size fractions can be collected.[2,3]

Existing cascade impactors have certain disadvantages from the point of veiw of compatibility with the X-ray fluorescence analysis measurements. One problem is particle blow-off resulting from the rapidly moving air stream; as the particle deposition on the substrate increases, particles tend to be blown off the impaction surface and deposited on succeeding stages. Another problem is the finite probability for a particle to bounce off the surface on impact. Remedies, such as coating the substrate with a sticky substance, are only partially successful in preventing bounce-off and might interfere with subsequent elemental analysis. The particle deposits in these impactors are necessarily in the form of an image or images of a small slit or circular holes which are not ideal for subsequent elemental analysis of the samples by X-ray fluorescence.

The objective of the present program is to design an air sampling system which can automatically acquire size-fractionated air particulate samples in a form compatible with X-ray fluorescence analysis, while at the same time avoiding particle bounce-off difficulties. Initial specifications call for the ability to separate particles into two size ranges corresponding to particles above and below a cut-off at 2 micron particle diameter. This represents the minimum in the distribution of total volume vs. particle size curve observed in the so called bimodal distribution of urban atmospheric aerosols.[4] The design will permit later extension to three or more size ranges. Measurements performed on the prototype size fractionator include collection efficiency and loss as a function of particle size.

The complete sampling system will be capable of automatic acquisition of a series of samples with adjustable sampling periods of 1 to 24 hours. The calibration and reliability of the prototype device will be suitably tested. Since it is likely that a number of duplicate systems will be required for the St. Louis RAPS program, extensive documentation will be required to allow large scale production of the final model.

B. Approach

A brief survey of particle sizing methods was necessarily a preface to the design phases of the program. Various mechanisms for the physical separation of particles according to size were studied and their advantages and limitations outlined. Possibilities included electrostatic, thermal, acoustical and optical methods in addition to the aerodynamic methods discussed earlier. These studies eventually related to the more fundamental problem of the definition of particle size. Since, in general, the shape, density, dielectric properties, etc. of the particles in the atmospheric aerosol are unpredictible, the interpretation of the term "particle size" depends on a large degree to the method of measurement. However, in any foreseeable atmospheric aerosol studies, the questions of most interest concern effects such as the mobility of the particulates in the atmosphere and their uptake and retention through respiration. In these contexts the most relevant definition of particle size relates to the aerodynamic size of the particle which governs its motion in these

situations. These considerations lead to the conclusion that separation methods based on aerodynamic effects most nearly measure the important parameters. Present methods of particle size measurement and the associated terminology reflect this bias. Since none of the alternative methods of particle sizing exhibits unique advantages over the aerodynamic method, we conclude that the adaptation of the latter would be appropriate.

C. Progress and Results

At the start of this program it was obvious that use of a normal impactor, in which the heavier particles impact and collect on a surface, cannot conveniently provide samples suitable for X-ray fluorescence analysis on large numbers of samples. Consequently emphasis was immediately placed on a "virtual" impactor scheme which results in separating the particles into two airstreams according to their size. Each airstream could then be passed through a filter to provide particulate samples in the ideal form for X-ray analysis. Since Environmental Research Corporation (ERC) had supplied a particle-size fractionator to EPA based on these general principles, the evaluation of this unit, described in the following sections, was carried out prior to developing a better unit. The study was designed to determine the separation characteristics and losses of the unit as a function of particle size and to relate these characteristics to critical design parameters. This information could then be used to assess the practicability of large-scale use of this principle in air samplers.

1. Description of ERC unit

Figure 1 is a phtotgraph of a disassembled ERC virtual impactor showing the various components, and Fig. 2 is a simplified assembly drawing.

The aerosol is drawn through the three entrance holes in the part labeled B (in Fig. 2) at a total rate of 50 ℓ/min. The diameter of the holes in parts B and F are 3.96 mm and 2.18 mm while the "impaction distance" to jet diameter ratios are 0.45 and 0.75 respectively for the two separating stages. The corresponding Reynolds numbers for the jets are 5900 and 1500. The combination of the hole in part F and those around the flange on part E distributes the internal flow such that only one seventh of the total flow is allowed through the inner tube E. Particles which cannot negotiate the turns around the lips of the protruding tubes in part D will be carried down into the inner tube. The process is repeated in a similar fashion at the lower section of the apparatus where the flow through tube K is maintained at 1 ℓ/min. Thus filter A will collect large particles above the 2 micron size cut together with about 2% of the small particles. Most of the small particles will be carried by the main flow at 49 ℓ/min and be collected on filter B.

2. Loss measurement method

Due to the close approximation of their geometric diameters to unit density Stoke's diameters, dioctyl phthalate (DOP) droplets, having a specific gravity of 0.98, are well suited to serve as test particles. They are generated by a Berglund-Liu monodisperse aerosol generator. Uranine (fluorescein sodium) is used as a tracer for quantitative measurements, particle losses at various points within the impactor being

determined by washing off the aerosol deposition from a particular region of interest. The uranine content of the resulting solution is then measured by UV fluorescence techniques.

Figure 3 is a schematic of the UV fluorescence analyzer. A 76-mm diameter pyrex dish holds the sample solution. The central portion of the solution is viewed by a photomultiplier via a mirror so that edge effects and UV attenuation in glasswares are avoided. The signal-to-background ratio is greatly enhanced by the use of complementary filters, one at the mercury light source with a transmission band from 2500A to 4000 A and the other (green X1) in front of the photomultiplier. This scheme also renders measurements practically immune to UV scattering by dust or DOP itself. The filter combination is not optimized for maximum sensitivity but rather it yields an adequate and convenient operational level. The stability of the analyzer is monitored with the aid of fiber optics in order to maintain a fixed source-detector transfer function which is checked before and after each measurement by means of a sliding shutter.

3. Experimental procedure in loss measurement

The virtual impactor must be operated vertically since gravitational effects are not negligible for large particles in regions of low flow rate. A carbon vane pump (Gast #0522-103-G18D) operating at 1725 rpm is used. The total flow rate of 50 ℓ/min is monitored with a manometer which is calibrated with a temperature-compensated integrating flow meter. The rate through filter A is maintained at 1 ℓ/min by an inline flow meter.

DOP particles of 1 to 10 micron diameters are produced by a Berglund-Liu monodisperse aerosol generator in which a liquid jet is produced by forcing a solution of the particulate matter in a volatile solvent through an orifice with a syringe pump. A periodic disturbance is imparted to the liquid jet by vibrating the orifice with a piezoelectric ceramic. Operating in the proper region of instability of a liquid jet, the eventual size of the particle depends on four influencing factors:

i) The feed rate of the syringe pump.

ii) The vibrational frequency of the orifice.

iii) The concentration of non-volatile solute.

iv) Any voids occurring in the residual particle when the solvent in the original droplet evaporates.

For consistant operation, a single calibrated feed rate of 1.3307×10^{-3} ml/s and a vibration frequency of 144.60 KHz are used to generate initial droplets of 26 microns with a 10 micron orifice. The solutions used consist of one part by volume of demineralized water to 14 parts of isopropryl alcohol with 50 µg/ml of uranine and selected amounts of DOP according to the final particle size desired. The droplets are dispersed and dried during mixing with a dry airstream. They are charge neutralized by exposure to a 10 mc Krypton-85 source. Uniformity of the aerosol is checked by visual observation of the initial droplet stream as deflected by a transverse air jet. With the aid of a scanning electron microscope, samples of individual particles are also examined occasionally for size and void fraction estimations.

Since the sizes of small particles are significantly affected by the amount of impurities present in the solution, the syringes are

regularly ultrasonically cleaned with detergents followed by water and alcohol rinses. Impurities in the DOP solution are thereby limited to about 10 μg/ml of alcohol residue and 50 μg/ml of uranine.

For each test run, the loss profile is determined from washings of depositions from six designated regions: (1) parts B and C, (2) part D, (3) the inside wall of tube E, (4) parts F and G, (5) part H, and (6) part K. A very slight loss also is known to occur in connecting tube to filter B. Uranine, being very soluble in water, is retrieved readily from the depositions on 0.8 micron Millipore filters. For DOP droplets greater than 5 microns, a few seconds of ultrasonic agitation will facilitate complete retrieval.

4. Results on ERC impactor

A number of calibration and monitoring functions were checked to minimize instrumental errors. The average air sampling rate as determined from total integrated flow for all the test runs is 49.75 ℓ/min with an rms deviation of 1.2%. Note that this represents the stability of the sampling rate with no feedback control, following initial adjustment to allow for different filters. The average feed rate of the syringe pump is 1.3307×10^{-3} ml/s with an rms deviation of 0.3% for different syringes. The orifice vibration frequency is continuously monitored and exhibits less than 0.1% deviation from its mean value of 144.60 KHz. With careful preparation of solutions used for generating aerosols, the overall error on the particle size is probably 1% in all cases except for the rare case where the impurities become a dominating factor.

Since the absorption and emission bands of fluorescein sodium partially overlap each other, the effect of self-absorption becomes significant and must be corrected for when using concentrated solutions. Figure 4 shows a plot of detector output current vs. uranine concentration obtained with seven dilutions of a common sample. A least-squares fit to the calibration data gives

$$I = 0.4723 (1-\exp (-42678x))$$

where I is the photomultiplier anode current in microampere and x is the uranine concentration in g/cm^2. A constant background of 5.6×10^{-10} amp is subtracted from each measurement. This yields an effective attanuation length of 58.43 $\mu g/cm^2$ defined as the concentration at which 63% of the radiations is absorbed. The detection limit at 95% confidence level is 1 ng/cm^2, corresponding to approximately 10 ng in the sample. A typical test run collects about 10 micrograms of the tracer; at such level self-absorption has no significant effect.

Table 1 is a summary of the percent deposition of DOP on various parts of the sampler and filters for incident particle sizes between 1 to 10 microns. The particle sizes are expressed in terms of unit density Stoke's diameters. They include corrections for 50 µg/ml of uranine and 10 µg/ml of solvent residue which are taken to have a bulk density of 1.7 g/ml, and also for an estimated void fraction of 48% as determined by scanning electron microscope observations. The 1.06 micron particles consist of mainly uranine with no DOP.

EVALUATION OF ERC VIRTUAL IMPACTOR

PERCENT DEPOSITION OF MONODISPERSE DOP ON SAMPLER AND FILTERS

UNIT DENSITY STOKE'S DIAMETER	1.06 (µm)	1.26 (µm)	1.63 (µm)	2.08 (µm)	2.55 (µm)	3.04 (µm)	4.02 (µm)	6.01 (µm)	8.01 (µm)	8.63 (µm)	10.00 (µm)
REGION 1	4.7	4.1	10.2	11.8	9.2	0.4	0.2	0.8	2.0	2.6	4.6
REGION 2	0.1	0.2	1.3	3.2	15.3	21.9	1.2	0.1	0.6	0.4	0.8
REGION 3	0.1	0.1	0.2	0.1	0.2	0.1	0.1	0.2	0.7	0.6	1.2
REGION 4	1.8	2.9	2.0	0.9	0.9	0.7	1.1	3.2	1.6	2.4	3.5
REGION 5	0.1	0.4	11.0	8.9	0.8	0.1	0.7	0.7	2.5	8.0	32.4
REGION 6	0.1	0.2	0.2	0.2	0.5	0.4	0.5	1.2	1.9	1.6	1.7
TOTAL LOSS	6.9	7.9	24.9	25.1	26.9	23.6	3.8	6.2	9.3	15,6	44.2
FILTER A (Above Cut)	4.2	4.7	11.5	26.3	49.5	75.1	95.7	93.5	90.2	84.0	55.3
FILTER B (Below Cut)	88.9	87.2	63.5	48.7	23.5	1.3	0.4	0.3	0.5	0.4	0.4

TABLE 1

Figure 5 is a graphical illustration of the overall results. The structure in the loss spectrum is derived from the composite of its various smoothed components. The loss spectrum due to a single contributing mechanism is expected to have a smooth variation with particle size.

Figures 6 through 11 are the plots for the six loss regions. It is observed that for region 1, the peak at small particle sizes is due to the ring shaped deposition around the holes on the underside of part B, as can be seen in Fig. 1. Such depositions are believed to be the results of direct impaction from the radial spatial oscillation of the streamlines rather than from eddy depositions. The oscillation is characteristic of the local geometry and flow rate. Similar phenomena have been observed in rectangular impactors where a succession of line deposits appear about an impaction slit.[5] We note that one of the three supporting legs on part D in Fig. 1 is narrower than the others. The presence of these legs in the most direct line of flow has a definite bearing on the balance of flow rate in the individual channels. Consequently, there is usually no ring deposit around the hole opposite to the narrow supporting leg, but a higher loss is found on the edge of the corresponding opening in part C. The losses at larger particle sizes are from the depositions on the upper lips of the entrance holes.

Depositions in region 2 are found mostly on the lips of the protruding tubes of part D. The impaction depositions show distinct azimuthal variations, reflecting the sensitivity of flow patterns to structural asymmetries. Part C is used to reduce the eddy losses around the tubes but some deposition is found on its circular openings.

For region 3, there is evidence that the expanding jets touch upon the adjacent walls on part E. The slightly higher loss toward larger particle sizes probably reflect the higher penetrating power of the more massive particles through the boundary layers near the walls.

Losses in region 4 have the same nature as those in region 1. The shifting of the loss peak to a smaller size indicates that the characteristic size cut of the second stage of separation is somewhat lower than that of the first stage. The data point at 6 μm is believed to be an anomaly; this is also obvious from its deviation from the expected smooth collection curve for filter A.

The loss spectrum for region 5 should behave similarly to region 2. Besides the slight shift of the loss peak to the smaller size, which is consistant with the parallel comparison of regions 1 and 4, there is an overwhelmingly high turbulance loss component at large particle sizes when the flow through filter A is restricted to 1 ℓ/min.

There are no distinct patterns of deposition in region 6; most of the losses probably occur in the slight mismatch to the filter holder.

5. Summary of evaluation of ERC unit

It is obvious that the virtual impactor can successfully separate two size ranges of particles and collect them on filters.

High losses near the cut region are probably intrinsic to any virtual impaction scheme since a deflecting surface will behave as an efficient impacting surface at the critical particle size. Furthermore, the boundary condition which occurs at the rigid surface of a real impactor

cannot be fully realized by a collection hole. The Gaussian-like pressure profile across the impinging jet cannot be balanced by a uniform static pressure in the collection volume. Streamlines will therefore penetrate into the hole and be accompanied by a counter flow near the edges when the net flow into the (large) particle collection volume is restrained. We suspect excessive turbulance will be developed in a very confined region where such counter flow cannot be maintained. The development of such turbulance is probably responsible for the high losses at large particle sizes. On the other hand, a significant amount of loss is found to depend on details rather than on basic principles of a virtual impactor and these can possibly be eliminated by suitable attention to design and fabrication.

6. Work on new dichotomous sampler

These tests on the ERC unit show that the virtual impaction scheme is workable for a dichotomous aerosol sampler, assuming that a peak in the particle loss spectrum near the cut point is tolerable. We have pinpointed the sources of losses in the ERC model and expect to be able to minimize losses in the new design for the St. Louis RAPS study.

We have decided against the alternative sampling scheme of using a total filter together with an impactor after-filter for the following reasons: (1) it is much more complicated to provide twice the pumping capacity and to match the flow rates in the filter pairs, (2) the bounce-off and blow-off problems associated with impactors would require the added complexity of sticky and possibly rotating impaction surfaces, thus making the servicing of the instrument more difficult, (3) the virtual

impactor has two intrinsic advantages: namely, losses are reduced whenever bounce-off occurs and any blow-off phenomenon is of a second order effect in that only loss build ups are subjected to blow-off.

Based on the results on the ERC unit, we have designed and tested an improved version of the dichotomous sampler for use in the automatic air sampling station being designed for the St. Louis RAPS study. Improvements incorporated into the new design are as follows:

a) The sampler is designed for easy dismantlement; all sliding seals have been eliminated or replaced by compression seals.

b) Stainless steel construction is employed for mechanical integrity.

c) Inlet holes are streamlined to eliminate large particle losses in region 1. At 10 micron particle diameter, the losses in this region were reduced from 4.6% to only 0.1%.

d) Ring deposits around the back side of the inlet holes have been eliminated by recessing the surface where normal depositions occur. Losses have been reduced from 11.8% to only 0.1% for 2 micron particles.

e) The square lips of the protruding tubes are rounded to somewhat reduce the impaction losses on the lips.

f) The geometry in region 2 has been redesigned to minimize asymmetries in the flow patterns.

g) The internal flow division at region 2 has been measured to be 6.14:1. This ratio may still need to be optimized.

h) Region 3 is designed to have a conical flow section to minimize large particle settling at low flow rates. The inlet hole in region 4 is also streamlined. Losses at 10 micron are thus reduced from 3.5% to only 0.1%.

i) The ring deposit on the back side of the hole in region 4 is eliminated by recessing the surface. This means the elimination of the 2.9% loss peak at small particle size.

j) The size and shape of the hole in region 5 is optimized to reduce turbulent deposition of large particles which result in a loss reduction from 32.4% to 6.2% at 10 microns.

Preliminary measures indicate that total loss has been reduced from 42.5% to 11.0% at 10 microns, and a reduction of about 1/3 has been achieved in the small particle loss peak. A preliminary test of blow-off effect has been done on the new virtual impactor. We introduced 2 micron uranine particles into the airstream after the unit had sampled 234 m^3 of room air. By measuring any uranine collected on clean filters from subsequent pumping, we found the upper limit for blow-off to be 10^{-4}. We shall perform more thorough measurements when we finish all the detail changes on the prototype.

Further studies of the basic design of the virtual impactor are proceeding in parallel with design and construction of a prototype air-sampler. The final design of the virtual impactor will then be incorporated into the construction of the twelve automatic dichotomous air sampling stations required for the St. Louis RAPS program.

IV. PULSED X-RAY TUBE

A. Objectives

Previous investigations[1] have indicated that substantial improvements in system performance can be achieved by employing a pulsed excitation source operated synchronously with the X-ray spectrometer. By pulsing the X-ray tube on only at those times when the spectrometer is available for analysis of detected X-rays, pile-up effects are eliminated and a considerable increase in effective counting rate is achieved. Figure 12 is a schematic of the earlier pulsed system showing the operation of the prototype tube. A discriminator operating on the output of the X-ray detector triggers a grid pulse which shuts the X-ray source off for the duration of the analysis cycle; associated electronics turn the tube back on immediately after the preceeding event has been stored. In addition to eliminating dead-time and pile-up problems in the associated electronics, the method reduces the total average power requirements of the X-ray tube since the tube is operated only when the spectrometer system is sensitive. No current flows into the anode during the pulse processing time so instantaneous power levels many times higher than the average anode dissipation can be used when the tube is "ON".

Figure 13 is a plot of input-output counting rate characteristics, comparing the conventional excitation methods to the pulsed tube. Earlier data have indicated that effective counting rates of up to five times greater can be achieved by the pulsed method compared with conventional operation.

Although the prototype system[1] was adequate for demonstration of the basic method, the X-ray tube used in these preliminary experiments was unsuitable for extensive X-ray fluorescence analysis mainly due to inadequate electron emission from the directly heated tungsten emitter. The problem is further compounded when operating with a secondary fluorescence geometry such as is used in recent systems. A new design and development study is being carried out under the current contract to make the pulsed tube a practical approach for large-scale fluorescence analysis.

The X-ray fluorescence system delivered to the EPA as a result of last year's work exhibited typical detector counting rates of 5 to 10 Kc/s with its X-ray tube operated at 40 watts anode dissipation. This produced output rates of processed (i.e. free of pile-up) signals of only 4 to 6 Kc/s as a result of pile-up rejection. Using the same system in the pulsed mode would allow counting rates of 24 Kc/s of processed events with no pile-up losses, with the average X-ray tube power level below 100 watts.

Development of a new pulsed X-ray tube is being undertaken with the restriction that resulting design should be compatible with operation in the earlier EPA system. This boundary condition has a large effect on the design of the tube geometry and also affects the associated electronics. In particular, the electron optics must be designed to project a >100 mA beam of 30 to 80 keV electrons, into a 6 cm long 1/2 cm diameter anode tube to permit use of the close-coupled X-ray geometry as in the existing instrument. This beam must be turned "OFF" and "ON" with a timing uncertainty of less than 200 ns for full advantage of the pulsed mode to be realized. Since the close-coupled geometry necessitates a grounded-anode

tube design, pulsing must be performed at the negative high-voltage electron source, and must preferably be accomplished without fast switching of high voltages due to the proximity of the low-noise X-ray spectrometer electronics.

B. Tube Design

Although a number of methods of pulsing X-ray tubes have been considered, the decision has been reached to design the tube in the form of a planar triode structure with a thermionic cathode, low-voltage control grid, and high-voltage X-ray anode. The planar electrode design permits the generation of a uniform electron beam which can then be projected down the anode tube. One of the more important considerations is to avoid space charge limitations in the amount of current which can be transported in a narrow beam. In the following sections the design of the X-ray tube will be discussed in detail.

1. Cathode-grid assembly

The design of the high-current pulsed X-ray tube has been facilitated by the commercial availability of cathode-grid structures produced for microwave triodes. These large-area planar cathodes (typically 0.5 to 0.8 cm^2) are capable of peak emission current densities of 20 amps/cm^2. The grid-cathode spacings are 0.15 mm or less, allowing high-current switching with moderate grid control voltages. We have evaluated units from two manufacturers--one using an 0.8 cm^2 oxide-coated cathode, the other with a

0.5 cm^2 dispenser type cathode. Both cathodes need to be activated after pump-down of the tube and are "poisoned" by any subsequent exposure to atmosphere. The dispenser cathode can be reactivated, and has the additional advantage that it is less susceptible to damage from positive ion bombardment--an important consideration in X-ray tubes.

Although the difficulties attendant to using activated cathodes are serious, the alternative method of a directly-heated tungsten filament is out of the question due to power considerations. The activated cathodes operate at emission current densities of 10 amp/cm^2 with a filament power input of less than 10 watts; by contrast this emission level would require a power of several hundred watts in tungsten emitters. Based upon our earlier experience, the fact that the cathode is operated at a high negative voltage relative to the grounded anode imposes a practical limit of approximately 10 watts heater dissipation.

2. Electron-optics

Having defined the grid-cathode structure of the tube, we next consider the electron beam requirements. The principal question is whether adequate current can be projected within the beam dimensions in spite of space-charge effects. Referring to Fig. 14 we can consider the design problem in the following steps:

For a tube length of 10 cm from anode aperture to the X-ray target, and a maximum beam envelope radius, space-charge effects establish a maximum current which can be projected through this region at a given voltage.[6] This relationship can be expressed as

$$I = PV^{3/2}$$

where V is the potential of the beam relative to the tube and P is the perveance. Assuming a beam radius at entry of 0.25 cm and a tube length of 10 cm, then $P \cong 10^{-7}$ if V is in volts and I in amps. Thus the maximum currents which can be passed through the tube are:

0.48 amps at 30 KV

1.06 amps at 50 KV

6.82 amps at 80 KV

Since a peak current of 200 mA is sufficient for our application, these parameters are quite adequate.

The boundary conditions for maximum current flow through the tube define the focal length of the anode-cathode lens structure. The necessary focusing, correcting for the anode aperture lens effect, can be achieved by an arrangement of two concentric spheres of radius 2 cm and 4 cm respectively. The beam envelope is similar to the one illustrated in Fig. 14, and remains more or less constant over a wide range of current. The perveance of the focussing part of the lens structure is also approximately 10^{-7} so no space-charge limit to the current is imposed at this point. These electron optics appear to be capable of maintaining steady-state currents of 500 mA, or greater, over the entire operating range of the tube although in practice anode dissipation provides the limit to continuous operation.

3. Switching characteristics

Since the interelectrode distances, grid wire spacing, and cathode characteristics are known, it is possible to estimate the triode characteristics of the tube. The most important parameter initially is the amplification factor μ, defined as (V_{ANODE}/V_{GRID}) at the cut-off point. A low value of μ implies that a high negative grid voltage is necessary to cut off the anode current, necessitating the introduction of additional electrodes to reduce the field gradient at the grid. Calculations of μ appropriate for the triode structure of Fig. 14[7] yield an approximate value of $\mu = 3000$ corresponding to negative grid cut-off voltages of 12, 15 and 24 volts for plate voltages of 30, 50 and 80 KV respectively.

Calculations of plate current vs. grid voltage have been made for each of the above plate voltages assuming $\mu = 3000$. Results show that beam currents exceeding the space charge limits of the anode tube can be achieved and that these currents can be controlled at grid voltages well within the capabilities of transistor circuits. The switching speed of the tube is limited by the grid capacitance; electron transit times through the tube are of the order of a few nanoseconds. Assuming a grid circuit capacitance of 20 pF (the measured grid capacitance of the electron gun is 8 pF), then a pulse rise of 100 volts in 100 ns requires a current switching capability in the pulse driver of

$$I = \frac{CV}{\Delta t} = \frac{(20 \times 10^{-12})\ (10^{2})}{10^{-7}} = 20\ \text{mA}$$

which is well within the operating characteristics of typical transistors that might be used.

C. Electronic Design

The design of the associated electronics must contend with an assortment of problems not previously encountered in X-ray tube operation. For convenience we will consider the grid-pulse circuit separately from the X-ray controller. Although the X-ray tube characteristics outlined above appear to make the design of the grid circuit fairly straightforward, the problem is complicated by the necessity of maintaining the entire pulser circuit at the high negative cathode potential. The switching-speed requirement precludes the use of the high-voltage X-ray cable as a signal transmitting device since its capacity is excessive. Therefore it is necessary to attach the grid-drive circuits to the tube at its high voltage terminal.

1. Grid pulse circuit

Figure 15 shows such an arrangement whereby the dc power supply for the grid-drive circuit operates from the 6.3 V filament supply which is floating at voltages ranging from 0 to 100 KV dc. Control signals for the grid-circuit are optically coupled across the high-potential difference using LED and photodiode pairs. The components contained within the dashed region are all operated at the negative cathode potential. Signals are provided via the optical couplings to the control grid bias level, which determines the operating point according to the curves of Fig.16, and also an on/off control to determine the timing and duration of the beam current cut-off. Beam-current level in this system is determined by the grid bias instead of by the filament power control as in the earlier EPA system. The present design calls for the grid bias control amplitude to be transmitted

as a pulse duration rather than a variable voltage since the latter approach is sensitive to non-linearities in the optical isolation system. The on/off control signal can be utilized directly.

2. X-ray tube control loop

The full advantages of the pulsed mode of operation are only realized when the associated control circuitry maintains an optimum operating point for the system. The various operating conditions can best be discussed by considering the behavior of the system as the sample mass is increased, resulting in a corresponding increase of counting rate per unit of X-ray tube power. When the sample mass is small it is not possible to maintain high counting rates and the tube is operated at its maximum average power dissipation. For reasons to be discussed later, this is regulated by limiting the duty cycle of the tube and operating at maximum emission current during the ON period. This is effectively the same as operating continuously at maximum power since the probability of detecting one event per cycle is assumed small. In this first region of operation the power level is fixed by the maximum pulse beam current and maximum duty factor, and the counting rate varies linearly with sample mass. As the sample mass increases, the probability of an event during the ON period is increased to the point where a sizeable reduction in the average duty cycle would normally occur. However, this would decrease the average power dissipation so, in this second region, the instantaneous tube current can be increased to maintain the maximum allowable average power; the current increase compensates for the reduction in duty factor due to higher count rates. The magnitude of this effect increases with increasing sample

mass until a point is reached where the average ON time becomes comparable to the time required by the pulse circuitry to shut off the tube. The probability of additional pile-up events occurring during this time interval then tends to become significant. This constitutes the maximum counting rate limit for the system, further increases in sample mass in this region must be accompanied by a reduction in instantaneous X-ray tube power so that the pile-up probability in the tube shut off time does not become excessive.

The block diagram of Fig. 15 illustrates how these control features will be accomplished. The maximum ON time is determined by a preset one-shot which triggers a dead time interval when the preset ON time has been exceeded. This dead time interval is chosen according to the amplifier shaping times as defined in Fig. 13. The end of the dead time waveform then triggers the next ON period. This is the mode of operation at very low counting rates. As the counting rate is increased, the ON time one-shot is reset more frequently by pulses detected by the X-ray system. Thus the average ON time is reduced. This is the second region of operation during which the auxiliary feedback loop increases the tube current to maintain its average power constant. Meanwhile, a separate circuit is continuously monitoring the average duty factor and the desired minimum duty cycle is reached, this circuit causes an appropriate reduction in the pulse beam current as discussed for operation in the third region. Characteristic times for a typical system might be:

Dead time	50 μs
Maximum ON time	10 μs
Minimum ON time	2 μs

Since this feedback arrangement causes the pulsed tube system to determine its own operating point, normalizing data from one sample to the next is a different problem from that in the previous (conventional) system. The pulsed method of excitation used in this manner reduces dead time losses essentially to zero. Normalization of the counts can therefore be accomplished by feeding information on the integrated beam current during a count into the computer where the program performs the normalizing process.

D. Mechanical Design

The exterior design of the basic tube will be similar to the previous EPA tube design although its size is increased due to the larger cathode-grid structure used in the pulsed tube. Recent improvements in technique to be incorporated in the design include a ceramic high-voltage insulator and an electron-beam welded anode.

The grid-drive circuits will be contained in an oil-filled chamber attached to the rear of the tube. Although high-voltage insulation requirements will dictate a length of 25 cm or more for this section--the penalty of increased size is compensated by the improved cooling capabilities and much higher emission currents than in earlier designs. Optical isolation of the control signals will be accomplished via light pipes immersed in the oil bath.

E. Results

A prototype tube and associated electronic controls have been constructed and extensively tested with encouraging results. The basic mechanical design of the tube enclosure and desired lens structure was implemented with minimal difficulty. The tube is designed to be completely baked at 325°C with a 2 l/s ion pump attached for subsequent pumping of gases released by materials.

The electron gun used in the first attempt was of the dispenser cathode type with 0.5 cm^2 active area. (Eimac Y646B). The cathode was successfully activated and subsequent operating experience has not required reopening the tube. No observable deterioration in emission properties has been observed after approximately 100 hours of operation, mostly at 40 to 50 kV applied anode potential. Observations of the electron beam structure using X-ray imaging techniques indicate that the optics perform almost to the design specifications. The beam spot was approximately 5 mm diameter and remained relatively constant over a wide range of anode voltages and emission currents.

Measurements of plate (anode) current/grid voltage characteristics have been made and are presented in Fig. 17 for plate (anode) voltages of 30, 40 and 50 kV. The prototype design does not operate reliably above 50 kV due to marginal spacing within the oil filled tank (it is felt that the design requirements affecting the problem are well understood and that the final model will operate successfully at 80 kV). It is apparent from the curves that the maximum emission levels are adequate and that they can be easily controlled with the available grid voltages. A beam current of 100 mA at 5% pulse duty factor and 30 kV represents an average anode power dissipation of 150 watts.

The amplification factor (μ) based on the measured cut-off voltages is approximately 1700, compared to the value of 3000 calculated from the geometric factors. A more detailed analysis of the curves shows that they do not obey the usual triode current law,

$$I_p \propto (V_g + V_p/\mu)^{3/2}$$

expected from single theoretical considerations. This result can be explained by assuming a variable μ triode. In view of the larger cathode area and grid to anode spacing, and the overall configuration, it is reasonable to postulate that the effective area of the cathode increases with increasing anode voltage penetration through the grid. This would result in a steeper dependence of I_p on V_g than that of the above equation. Although there are possible adjustments in the lens configuration which could reduce this effect, no changes in design are anticipated since the departure from ideal triode behavior does not materially effect the pulse tube performance.

The switching characteristics of the triode have been determined and appear adequate. The grid circuit capacitance (including the high-voltage connector) were measured to be < 15 pF. The turn-off time for the system including detector response was < 300 ns. The ultimate limit on time response is set by the signal/noise ratio in the detector system and its effect on time resolution. Improvements in design of the pulser circuit could reduce the timing uncertainty to as low as 150 ns which would result in a further reduction in pile-up effects at the higher counting rates.

The total system performance has been measured in the feedback mode as a function of increasing sample mass and tube power. The basic control circuitry operated in the mode described previously with the exception that the maximum duty factor was determined manually instead of via feedback circuitry. One of the goals of the measurements was to determine the optimum ON time; the OFF period was 50 μs for all the data to be discussed.

Figures 18 and 19 are calculated curves based on the observed data from the rate measurements. Figure 18 is a plot of input rate vs. non-pile-up output rate for the case of two choices of maximum ON times; the turn-off time was assumed to be 300 ns. The performance for the 10 μs ON time (and larger times) is adequate; however, for the case of 2 μs ON, the pile-up probability is excessive even at moderate counting rates. From these type of data we can obtain a maximum allowable input counting rate based on a maximum acceptable pile-up probability. In the following discussion, we will assume a limit of 5% pile-up as maximum for useful analytical data. For 10 μs or longer ON times this occurs at approximately 17 kc assuming 50 μs OFF. If the timing uncertainty were reduced, the maximum input rate would more closely approach the theoretical imit of 20 kc/s for 50 μs OFF time. Further increases in counting rate limit can then be accomplished by going to shorter amplifier shaping times corresponding to shorter OFF periods for the X-ray tube. This can only be accomplished with some sacrifice in X-ray detector energy resolution.

Figure 19 is a plot of average and peak X-ray tube power vs. sample mass using the X-ray yield measured with the prototype tube. Also included is a plot of the output counting rate. The performance is as described

previously. In the region of small sample mass, the tube is operated at its maximum duty factor and corresponding maximum average power level. As the sample mass increases, the peak power increases to compensate for the increased dead time while maintaining the maximum average power. Finally the instantaneous counting rate is high enough for there to be a 5% probability of an event during the shut-off time, i.e. the 5% pile-up limit is reached. From this point on, the duty factor is fixed at some minimum value and the average power is gradually reduced while the count rate is maintained at the maximum value. The important benefits of the pulse mode of operation result from the fact that the tube is operated either at the maximum average power level with no power wasted during the system dead times or at the maximum allowable counting rate. The feedback loops thus ensure that the system operating in its best condition for a given sample size.

The quality of the spectra obtained with the pulsed tube is determined more by the secondary fluoresor geometry more than any electronic innovations which might be employed. Of greater importance is the question of the X-ray yield for a given tube current since the system is limited by X-ray tube power over much of its operating range. However, the ultimate test of the analytical system is the ability to measure the concentrations of elemental constituents with a high degree of sensitivity. For this reason we show in Fig. 20 a spectrum obtained on a 30 mg/cm^2 sample of NBS orchard leaves.

A Mo secondary target excited by Rh K X-rays was used for this measurement. The design of the anode structure was not optimum for secondary fluorescence efficiency and some increase over the measured yield is anticipated

in the final design. Nevertheless an output counting rate of 5 kc/s was achieved with 5 watts average anode power dissipation. The counting rate in these measurements was limited by the resolving time of the guard-ring rejection circuitry which was significantly greater than the X-ray tube switching times. This difficulty will be overcome in the final system.

F. Conclusion

The design and construction of the prototype pulsed X-ray tube has been completed. Tests show the system is capable of improved counting rate performance over a wide range of sample masses. With the incorporation of improved control circuitry and live time correction methods, the system will allow the analysis of wide range of sample types with automatic optimization of excitation conditions.

Experimental data obtained on the prototype tube have been sufficient to define the final design parameters for a complete analytical system. This second-generation energy-dispersive X-ray analysis system is currently being designed and will be completed for operation in the St. Louis RAPS program in 1974.

V. DIGITAL FILTER MARKING

After examining various techniques for marking digital computer-readable codes on the filter holders, we have chosen to use stick-on bar code labels (Monarch Marking Company). A standard bar code is employed in these labels and identifying numbers are printed to permit visual reading of the identification. The 37 x 9.5 mm area available on the filter holder permits a 12-digit marking--far more than required in practice. The bar code is read optically and existing hardware can be used to connect to the computer.

Digital readers will be installed on both the X-ray elemental analysis system and on the beta-gauging system. Samples will be moved by the sample changer into an intermediate position for digital identification before being moved to the measurement head where X-ray or beta-particle exposure occurs. The identification number of a particular filter will then be automatically associated with all the data acquired on that sample. This computerized bookkeeping capability is essential for error free analysis of the large number of samples anticipated.

VI. TOTAL PARTICULATE MEASUREMENTS

Preliminary tests with a prototype beta gauge have demonstrated the feasibility of measuring the total particulate mass accumulation during sampling periods of six hours or less. Assuming reasonable aerosol particulate mass concentrations, this would be equivalent to a detectible limit of 10 $\mu g/cm^2$ on filter substrates of 3 to 5 mg/cm^2.

Using a ^{147}Pm source and Si(Li) detector with appropriate counting electronics, we have performed a series of measurements on standard plastic thin films. Measurements of errors associated with reproducibility of the sample position and counting intervals indicate an accuracy of 10 $\mu g/cm^2$ is easily achieved in short counting intervals (30 seconds or less). Use of higher intensity radioactive sources could reduce this time even further.

A more serious concern in the measurement of particulates collected on membrane filters is the variation in mass of the substrate as a function of ambient relative humidity. A series of tests using different membrane filter types was performed to measure the error due to these humidity variations. Filters were cycled several times between 100% and 0% relative humidity and the reproducibility of their mass, after conditioning at constant humidity, was measured by direct weighing on a microbalance. The three types of filters were teflon, cellulose ester (Millipore) and polycarbonate (Nuclepore). The reproducibility of weight was best with the polycarbonate membranes--an average deviation from the mass of less than 0.5 ng/cm^2 for two samples cycled between the humidity limits four times.

The deviations for teflon were 0.8 $\mu g/cm^2$ and for the Millipore 6 $\mu g/cm^2$. All of these are well below the required accuracy of 10 $\mu g/cm^2$. However, the fact that the maximum weight changes with changes in relative humidity were of the order of 50 $\mu g/cm^2$ emphasises the importance of equilibrating the filters to a constant relative humidity before mass measurements. The final beta gauge design will include a provision for controlled humidity atmosphere, and the operating strategy will be designed to permit suitably long conditioning of filters before gauging.

REFERENCES AND FOOTNOTES

1. Jaklevic, J. M., Goulding, F. S. and Landis, D. A., IEEE Trans. Nucl. Sci., NS-19, No. 3, 392-395 (1972).

2. Andersen, A. A., Amer. Ind. Hyg. Assoc., 27, 160 (1966).

3. Lundgren, D. A., J. Air Poll. Cont. Assoc., 17, 225 (1967).

4. Whitby, K. T., Husar, R. B. and Liu, B. Y. H., "The Aerosol Size Distribution of Los Angeles Smog", Publication No. 159, Particle Technology Laboratory, University of Minnesota.

5. Berner, A., Private Communications.

6. Pierce, J. R., Theory and Design of Electron Beams, Van Nostrand, New York, 145 ff (1954).

7. Spangenberg, K. R., Vacuum Tubes, McGraw-Hill, New York (1948).

* Earlier Progress Report

Goulding, F. S. and Jaklevic, J. M., "X-Ray Fluorescence Spectrometer for Airborne Particulate Monitoring", Environmental Protection Technology Series EPA-R2-73-182, April 1973.

FIGURE CAPTIONS

Fig. 1. Components of the ERC virtual impactor.

Fig. 2. Simplified assembly drawing of the ERC virtual impactor.

Fig. 3. U. V. fluorescence analyzer.

Fig. 4. Self-absorption effect in uranine solution.

Fig. 5. Size separation characteristics and the total loss spectrum.

Fig. 6. Regional loss spectrum, Region 1.

Fig. 7. Regional loss spectrum, Region 2.

Fig. 8. Regional loss spectrum, Region 3.

Fig. 9. Regional loss spectrum, Region 4.

Fig. 10. Regional loss spectrum, Region 5.

Fig. 11. Regional loss spectrum, Region 6.

Fig. 12. Schematic of pulsed tube electronics.

Fig. 13. Input/output counting rate characteristics of pulsed tube compared to normal operation.

Fig. 14. Cross sectional view of electron optics used in pulsed tube.

Fig. 15. Schematic of control electronics for pulsed tube.

Fig. 16. Calculated plate current vs. voltage curves for prototype X-ray tube.

Fig. 17. Experimental plate current vs. voltage curves for prototype X-ray tube.

Fig. 18. Plot of input rate vs. non pile-up output rate for two different values of the maximum "on" time of the tube.

Fig. 19. Plot of X-ray tube power as a function of sample mass as automatically determined by the circuit of Fig. 15. The change in output counting rate is also shown.

Fig. 20. X-ray fluorescence spectrum of a sample (NBS orchard leaves) using the pulsed X-ray tube. The counting time was 400 seconds.

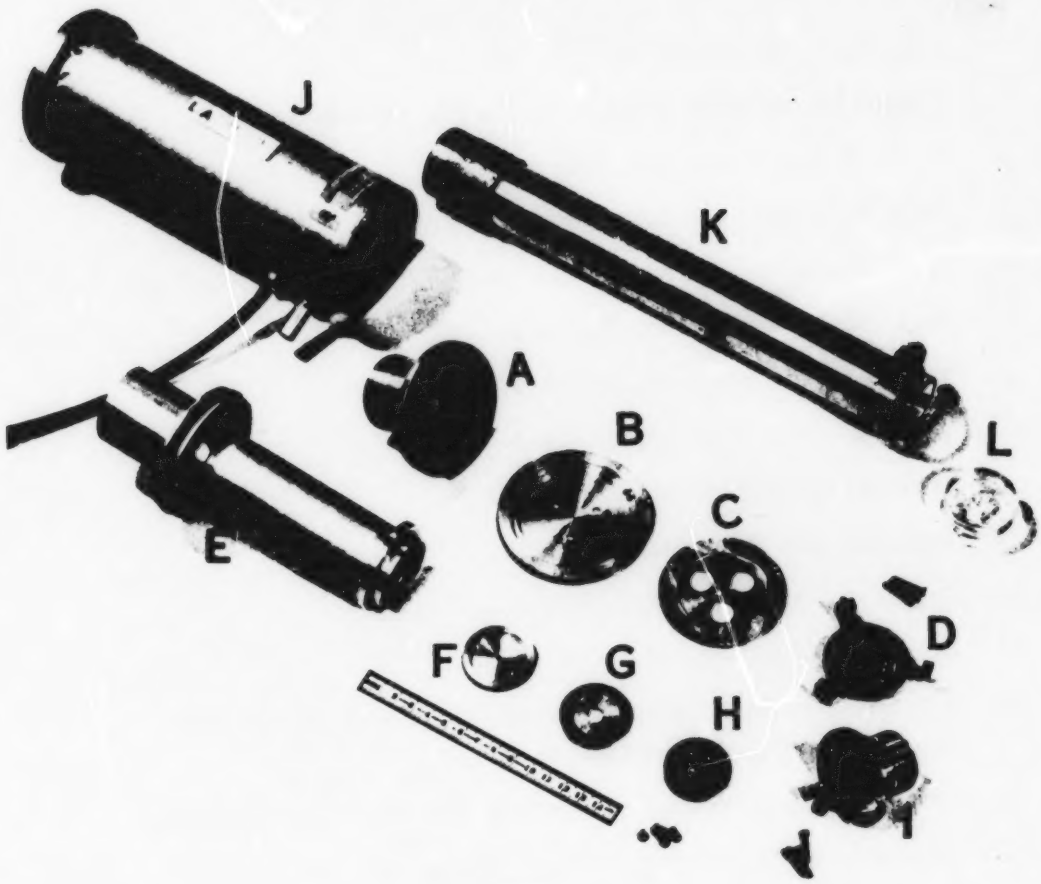

XBB 7311-6673A

Fig. 1

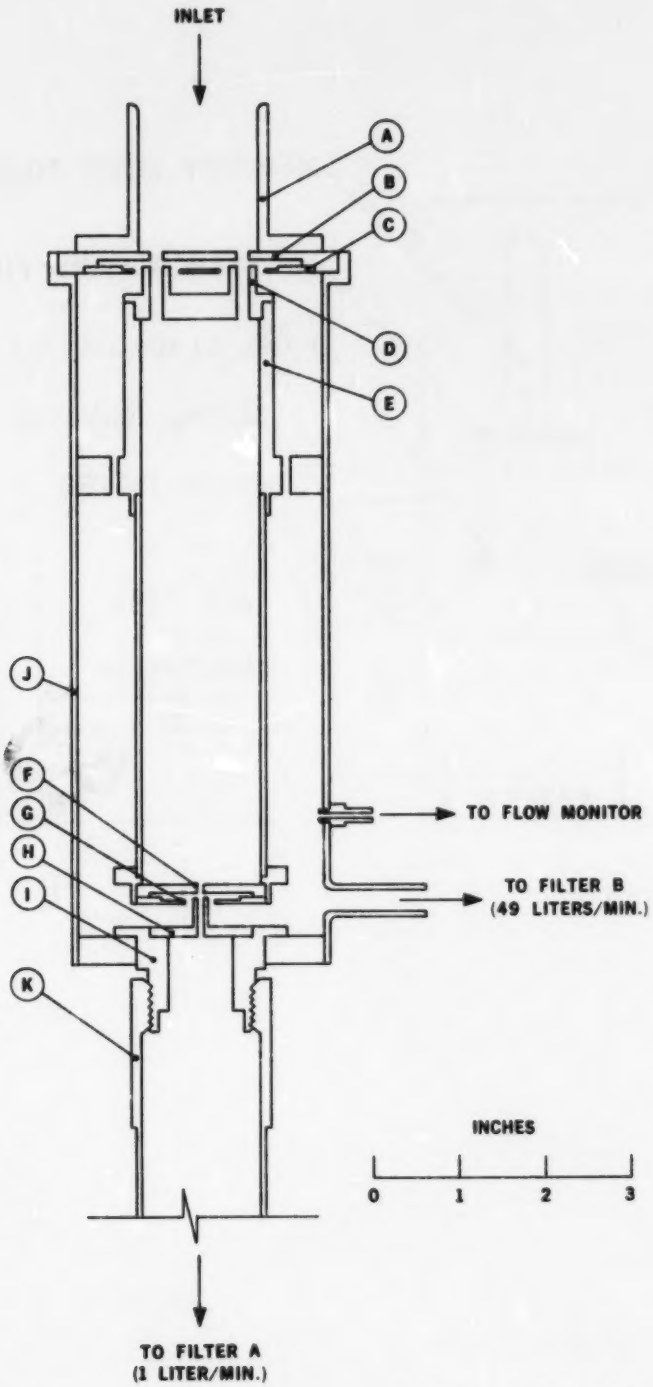

XBL 7311-6801

Fig. 2

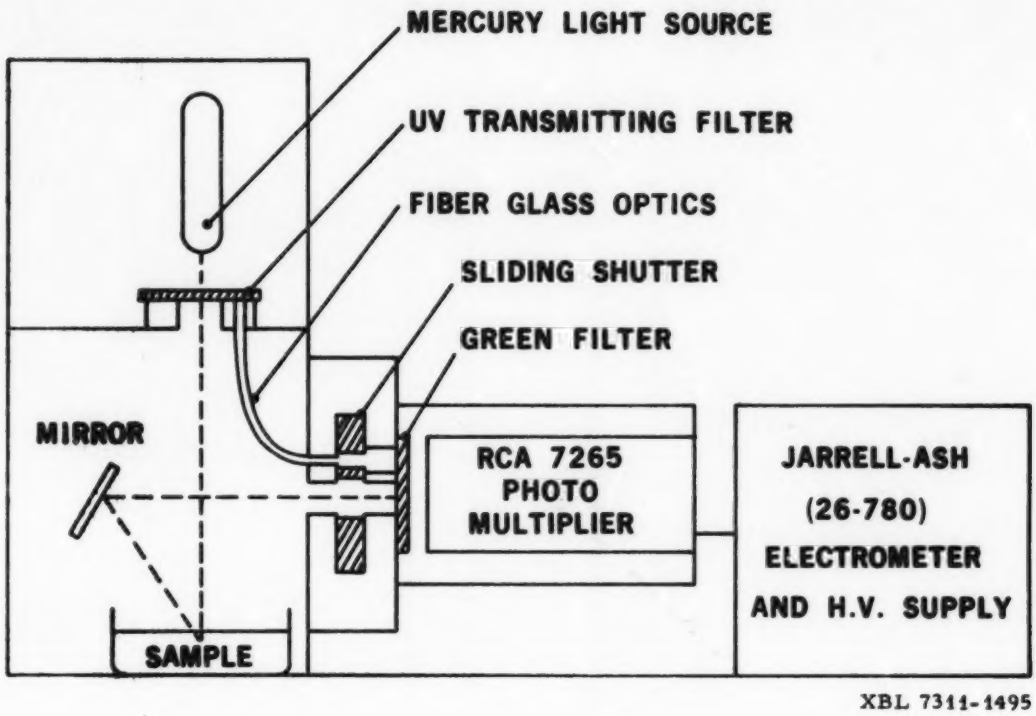
MERCURY LIGHT SOURCE
UV TRANSMITTING FILTER
FIBER GLASS OPTICS
SLIDING SHUTTER
GREEN FILTER
MIRROR
RCA 7265
PHOTO
MULTIPLIER
JARRELL-ASH
(26-780)
ELECTROMETER
AND H.V. SUPPLY
SAMPLE
XBL 7311-1495

Fig. 3

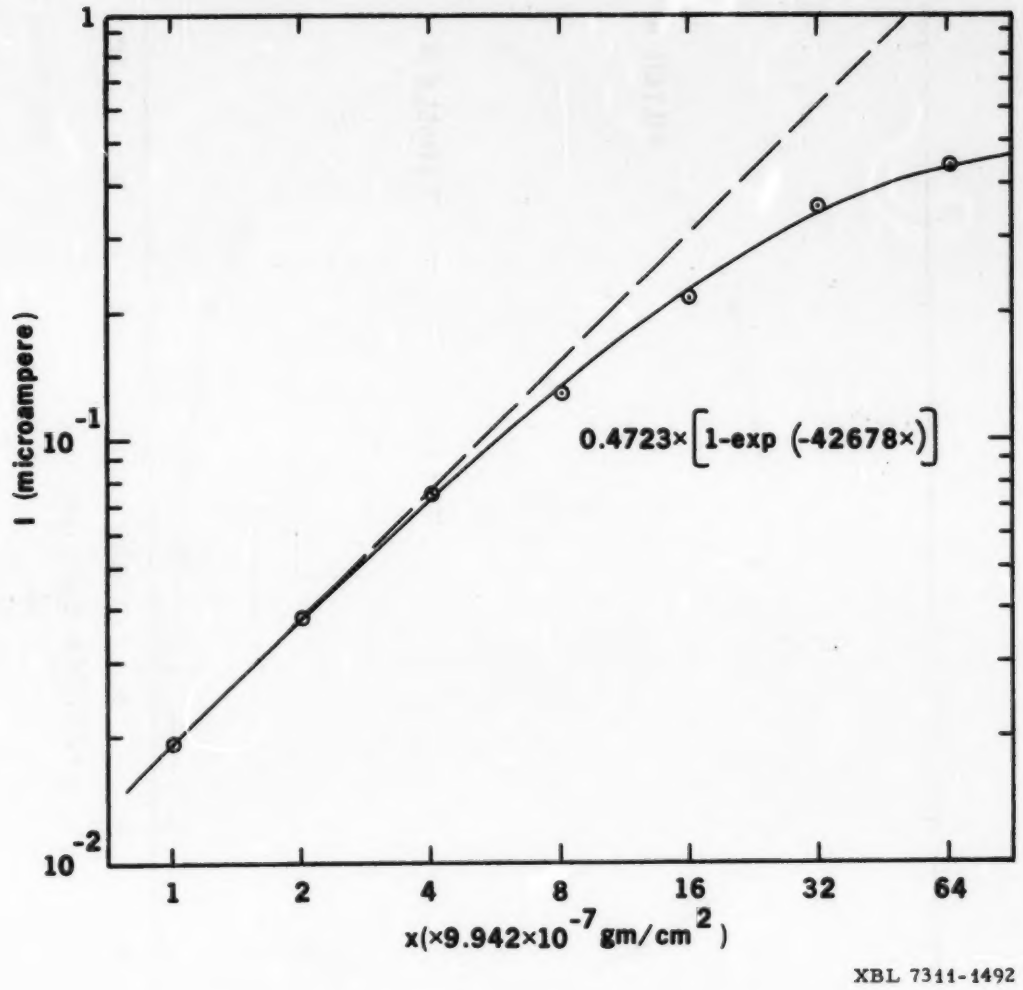
1
10^{-1}
10^{-2}
I (microampere)
$0.4723\times\left[1-\exp\left(-42678\times\right)\right]$
1
2
4
8
16
32
64
$x(\times 9.942\times 10^{-7}\ gm/cm^2)$
XBL 7311-1492

Fig. 4

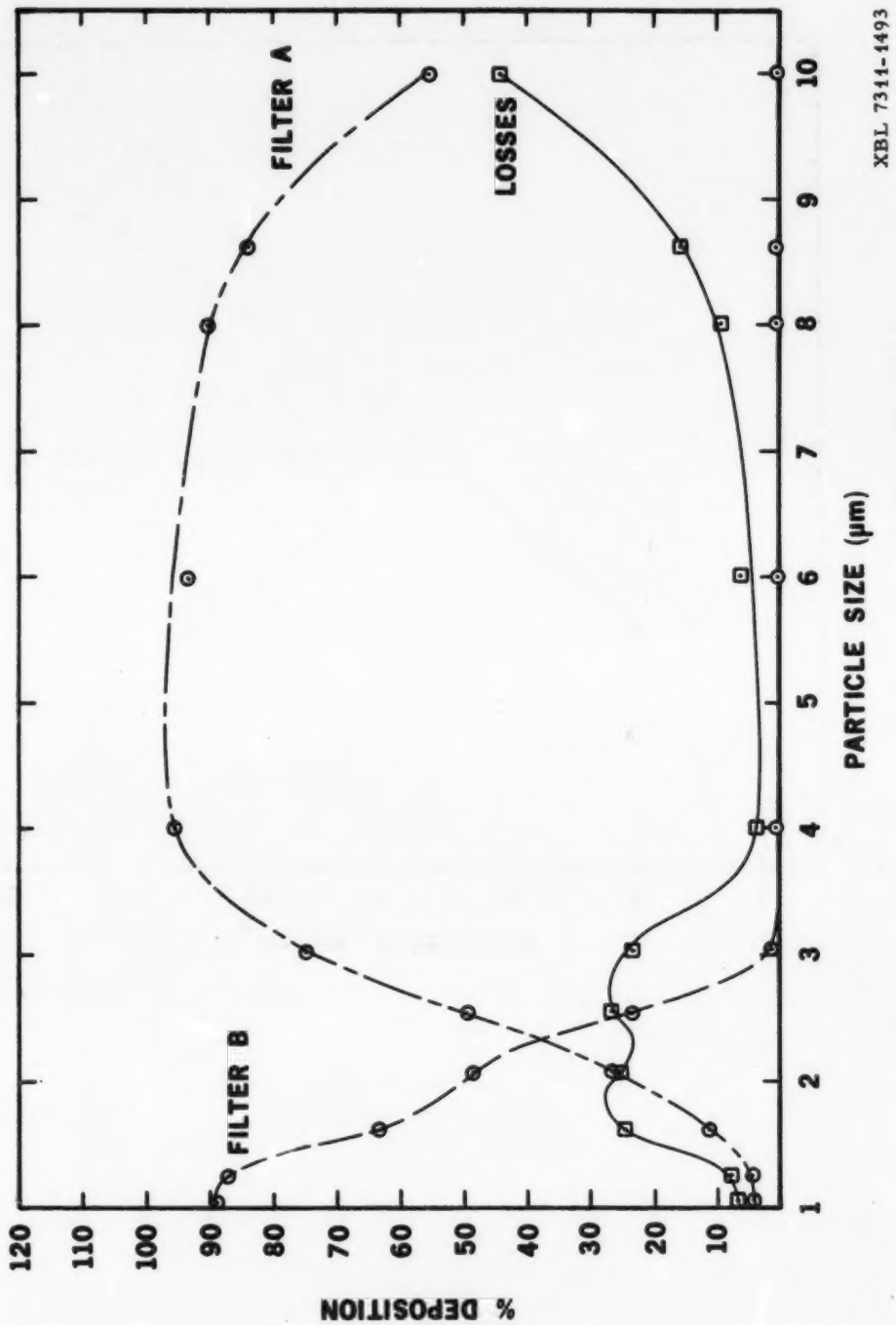

XBL 7311-1493

Fig. 5

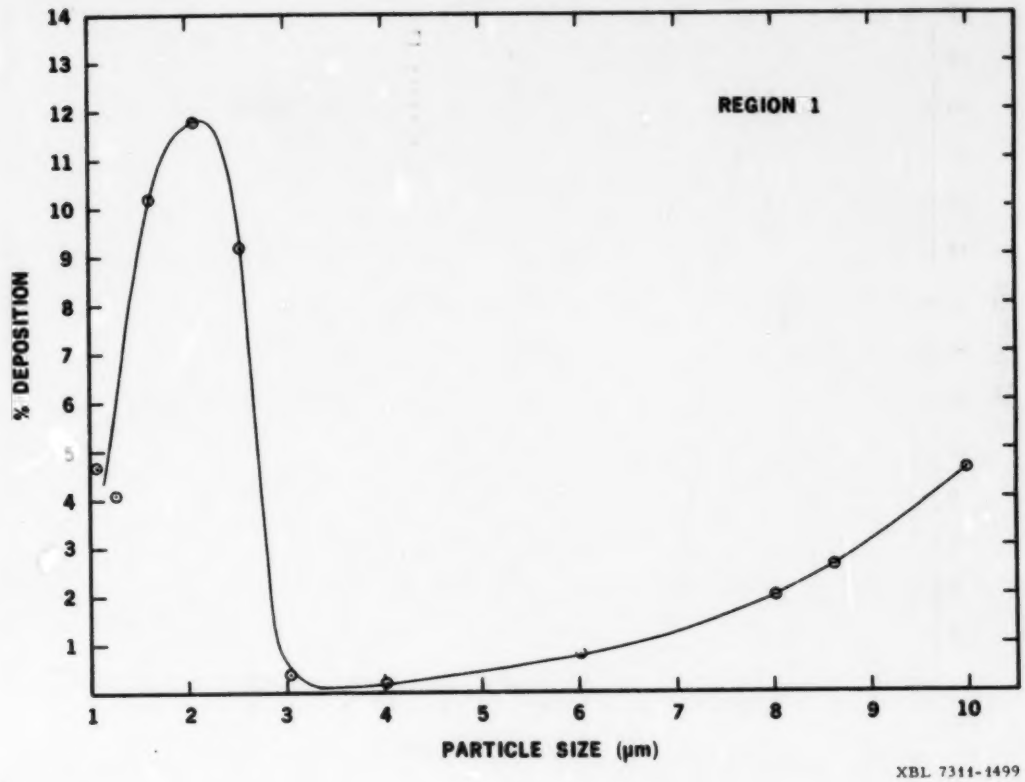

Fig. 6

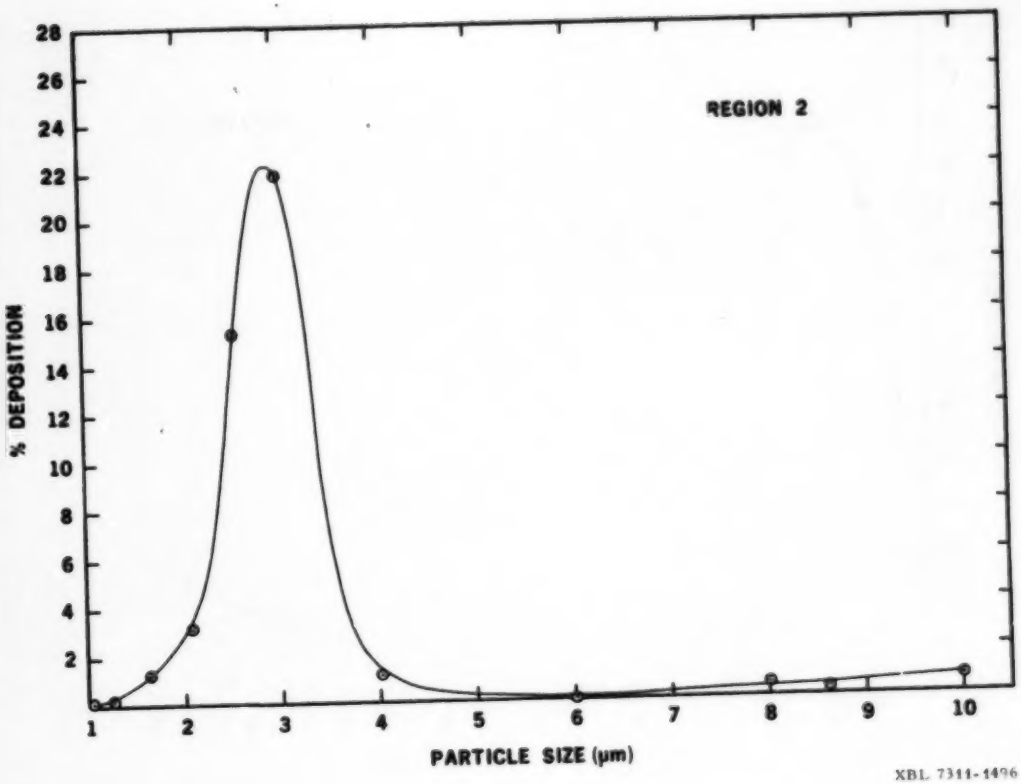
REGION 2
% DEPOSITION
PARTICLE SIZE (μm)
28
26
24
22
20
18
16
14
12
10
8
6
4
2
1
2
3
4
5
6
7
8
9
10
XBL 7311-1496

Fig. 7

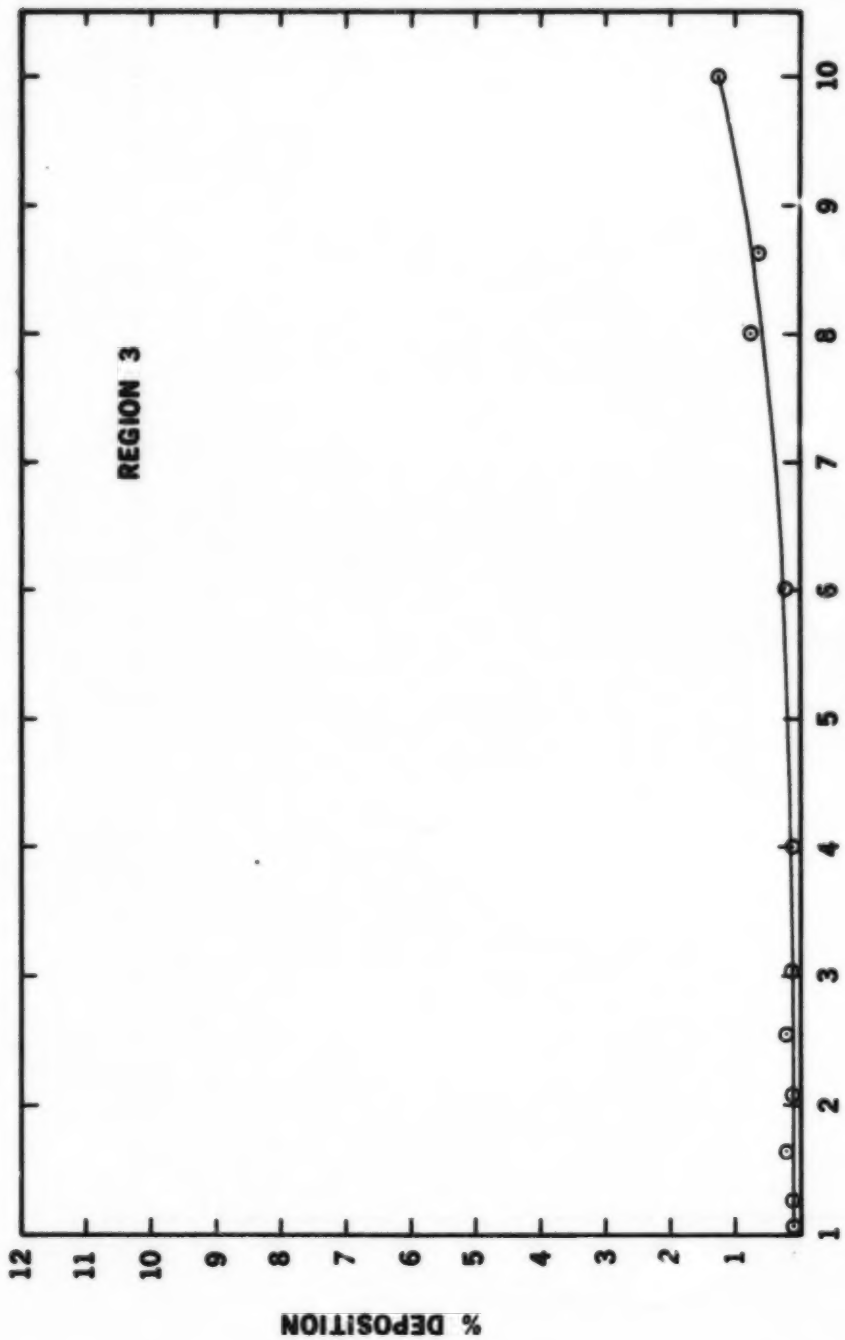

XBL 7311-1497

Fig. 8

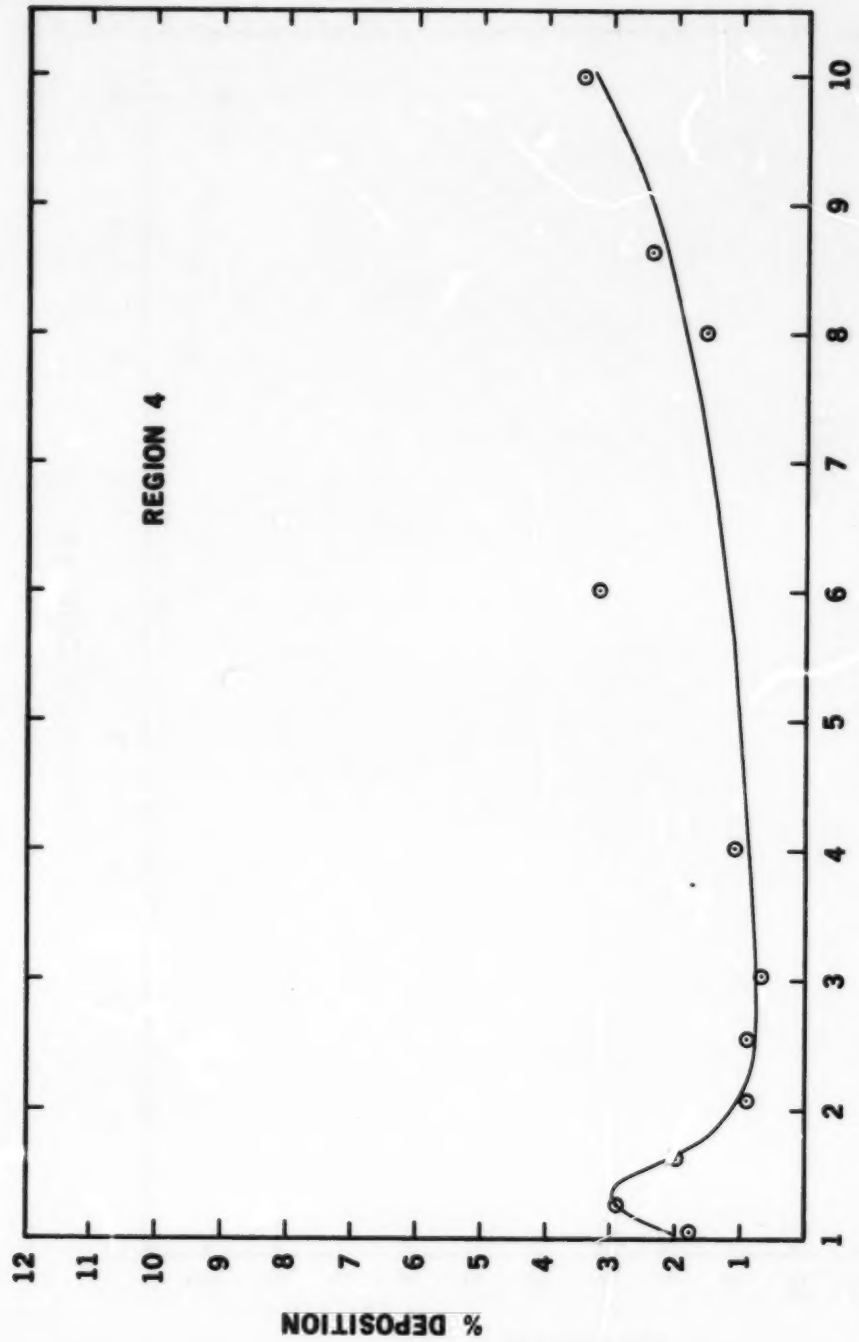

XBL 7311-1498

Fig. 9

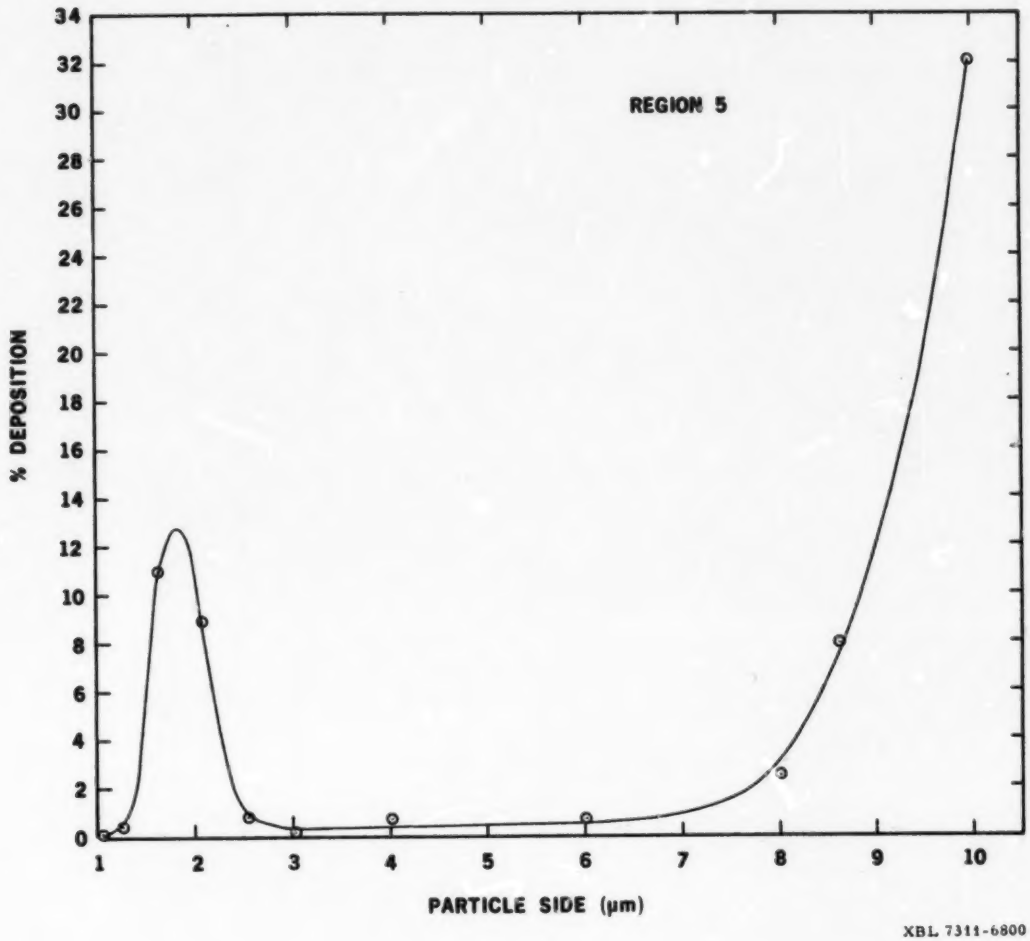
REGION 5
% DEPOSITION
PARTICLE SIDE (μm)
0
2
4
6
8
10
12
14
16
18
20
22
24
26
28
30
32
34
1
2
3
4
5
6
7
8
9
10
XBL 7311-6800

Fig. 10

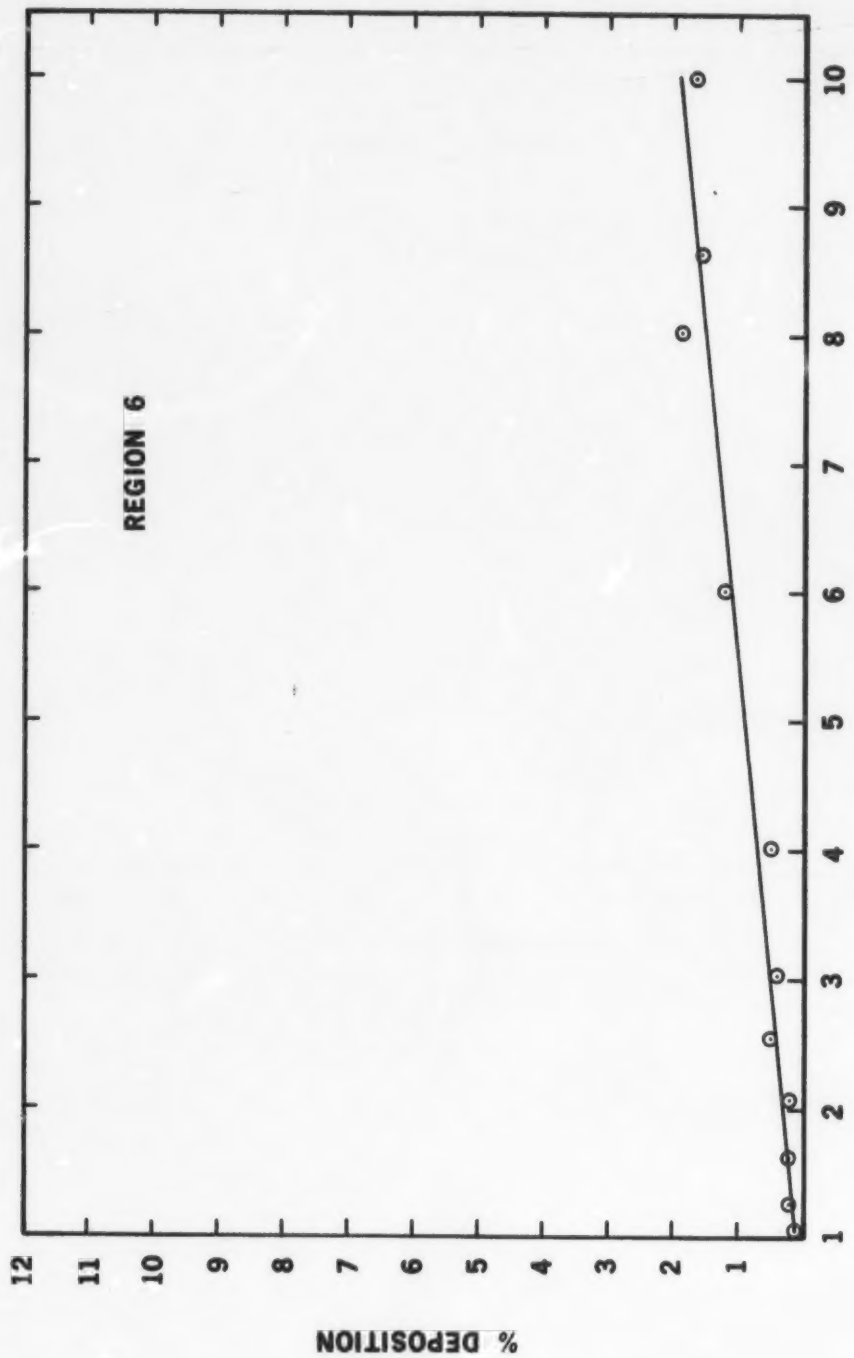

XBL 7311-1494

Fig. 11

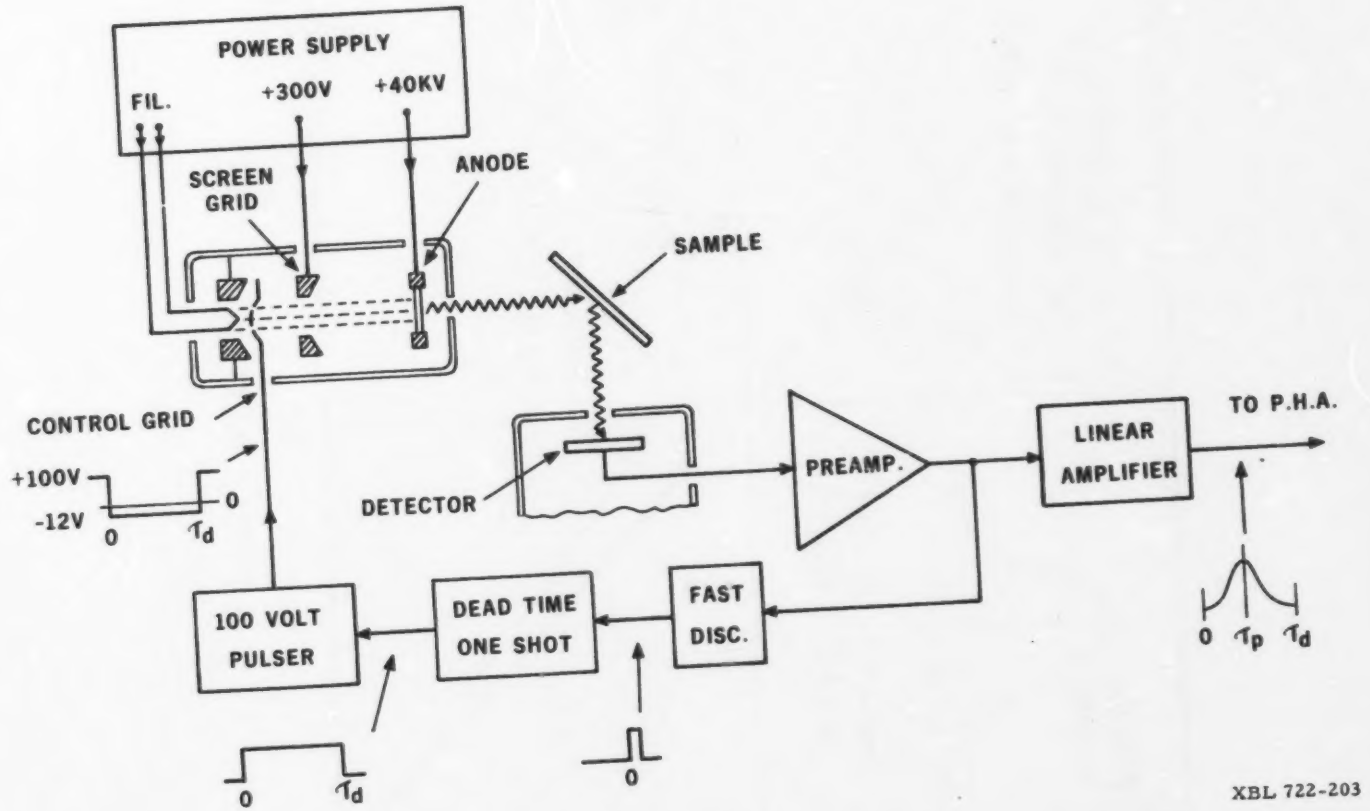
POWER SUPPLY
FIL.
+300V
+40KV
SCREEN GRID
ANODE
SAMPLE
CONTROL GRID
+100V
-12V
0
0
τ_d
DETECTOR
PREAMP.
LINEAR AMPLIFIER
TO P.H.A.
100 VOLT PULSER
DEAD TIME ONE SHOT
FAST DISC.
0
τ_d
0
0
τ_p
τ_d
XBL 722-203

Fig. 12

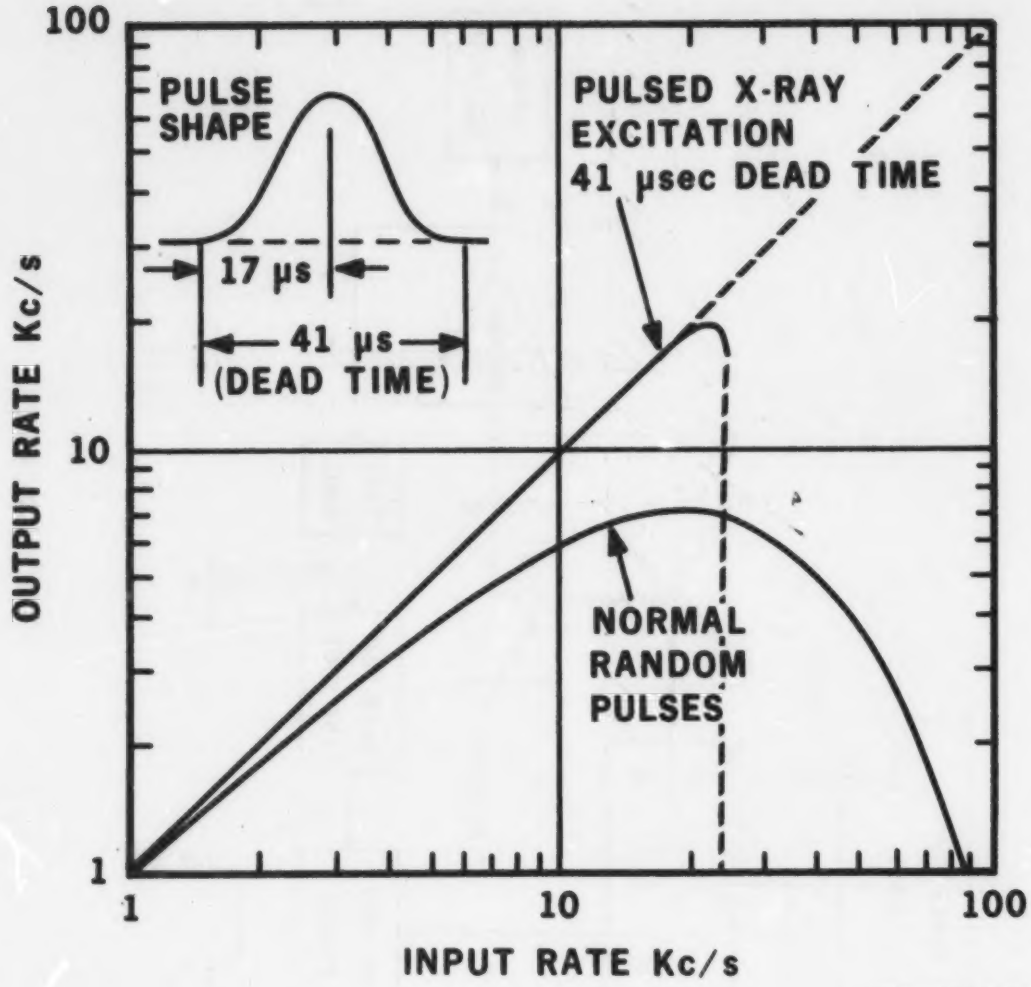

XBL 733-288

Fig. 13

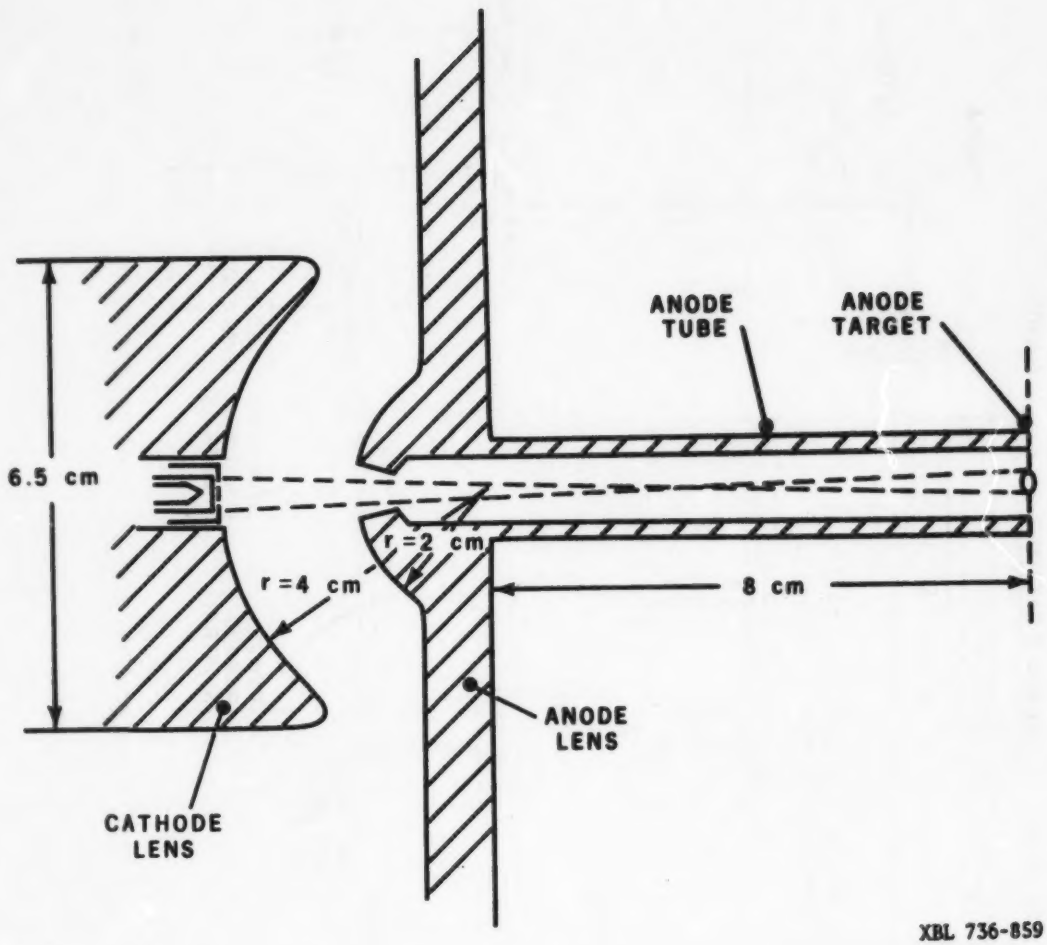
ANODE TUBE
ANODE TARGET
6.5 cm
r = 2 cm
r = 4 cm
8 cm
ANODE LENS
CATHODE LENS
XBL 736-859

Fig. 14

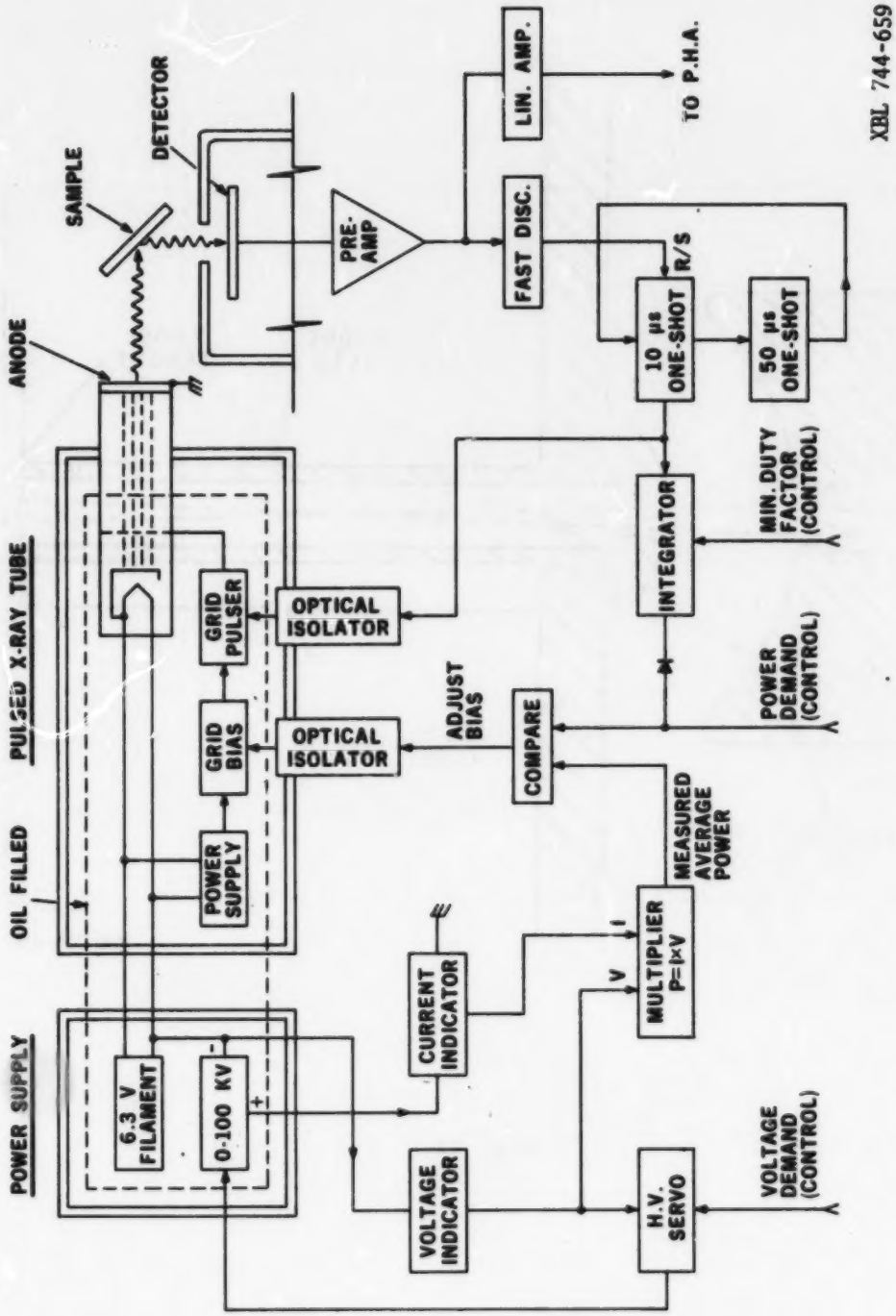
POWER SUPPLY
OIL FILLED
PULSED X-RAY TUBE
ANODE
SAMPLE
DETECTOR
6.3 V FILAMENT
0-100 KV
POWER SUPPLY
GRID BIAS
GRID PULSER
OPTICAL ISOLATOR
OPTICAL ISOLATOR
CURRENT INDICATOR
VOLTAGE INDICATOR
MULTIPLIER P=IxV
H.V. SERVO
VOLTAGE DEMAND (CONTROL)
ADJUST BIAS
COMPARE
MEASURED AVERAGE POWER
INTEGRATOR
POWER DEMAND (CONTROL)
MIN. DUTY FACTOR (CONTROL)
10 μs ONE-SHOT
50 μs ONE-SHOT
R/S
PRE-AMP
FAST DISC.
LIN. AMP.
TO P.H.A.
XBL 744-659

Fig. 15

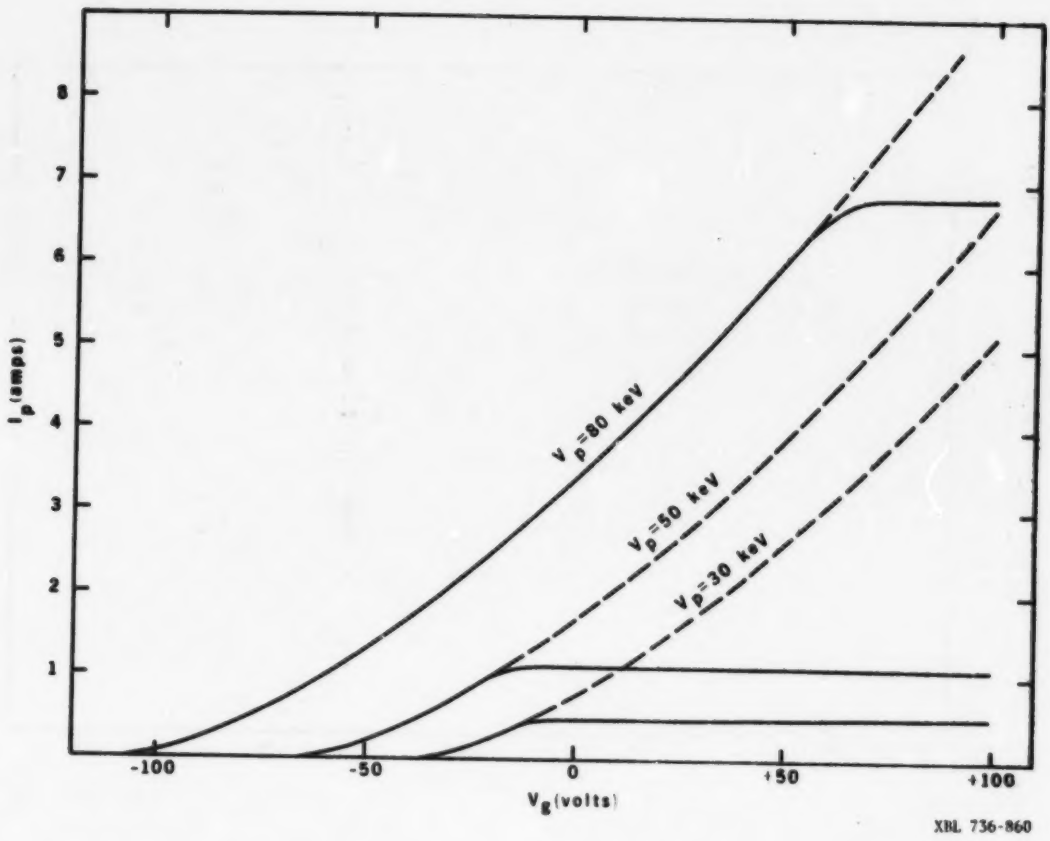
8
7
6
5
4
3
2
1
I_p (amps)
V_p=80 keV
V_p=50 keV
V_p=30 keV
-100
-50
0
+50
+100
V_g (volts)
XBL 736-860

Fig. 16

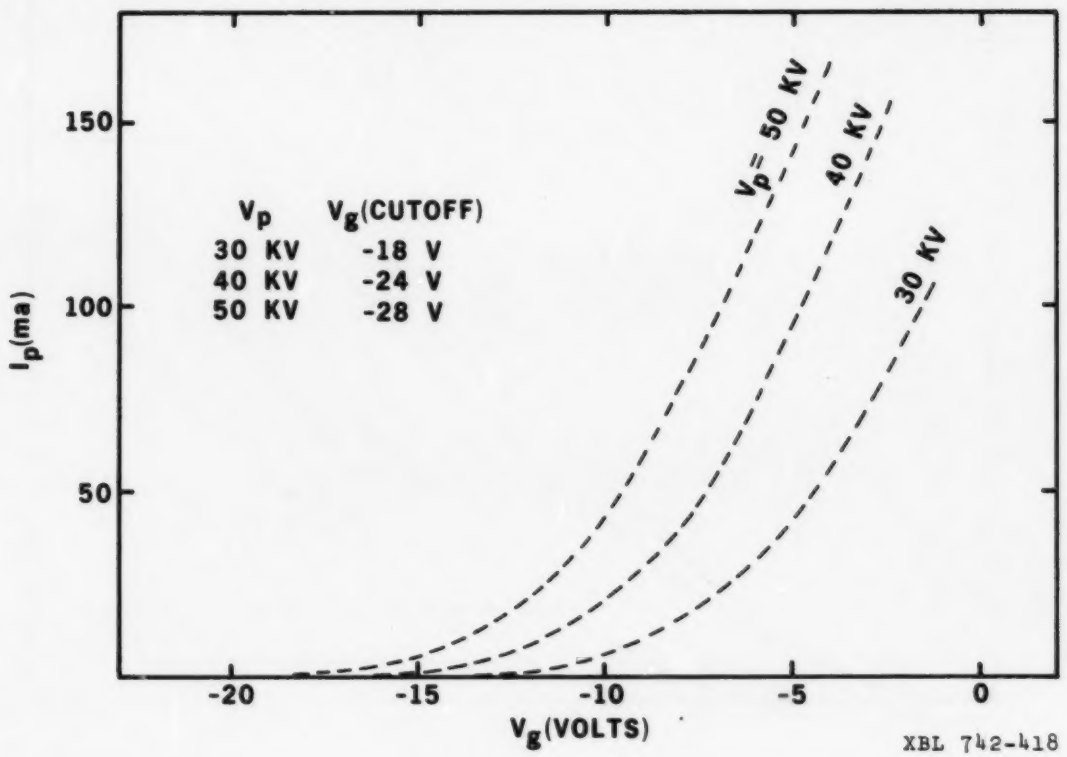
150
100
50
I_p(ma)
V_p V_g(CUTOFF)
30 KV -18 V
40 KV -24 V
50 KV -28 V
V_p= 50 KV
40 KV
30 KV
-20
-15
-10
-5
0
V_g(VOLTS)
XBL 742-418

Fig. 17

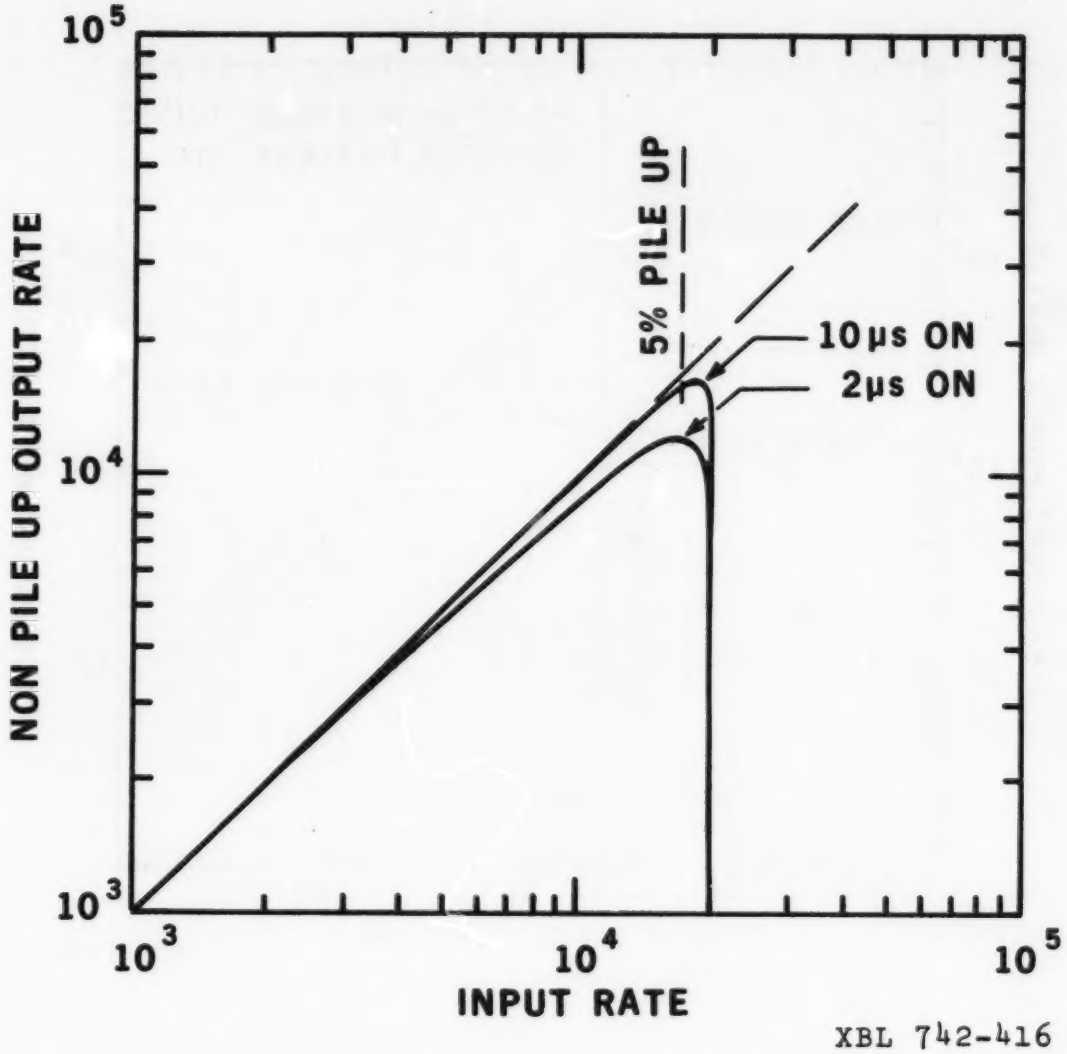
10^5
10^4
10^3
NON PILE UP OUTPUT RATE
5% PILE UP
10μs ON
2μs ON
10^3
10^4
10^5
INPUT RATE
XBL 742-416

Fig. 18

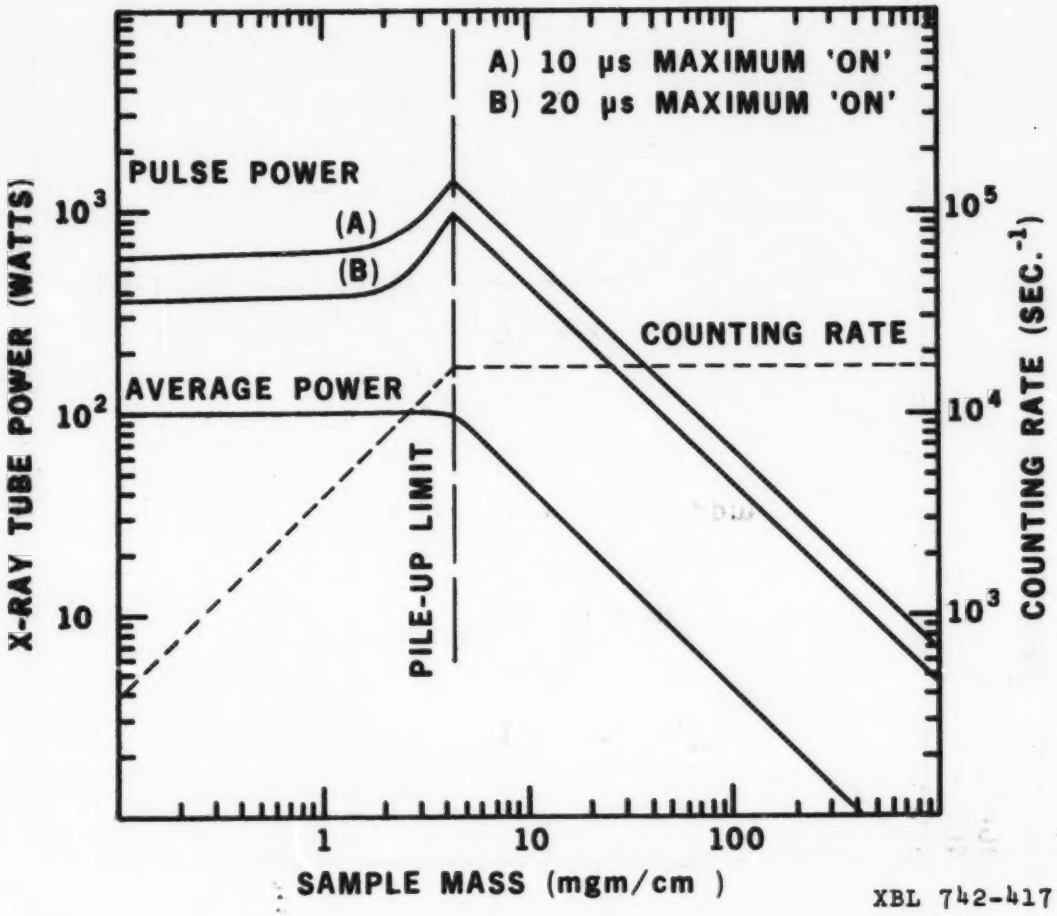
A) 10 μs MAXIMUM 'ON'
B) 20 μs MAXIMUM 'ON'
PULSE POWER
(A)
(B)
AVERAGE POWER
COUNTING RATE
PILE-UP LIMIT
X-RAY TUBE POWER (WATTS)
10³
10²
10
10⁵
10⁴
10³
COUNTING RATE (SEC.⁻¹)
1
10
100
SAMPLE MASS (mgm/cm)
XBL 742-417

Fig. 19

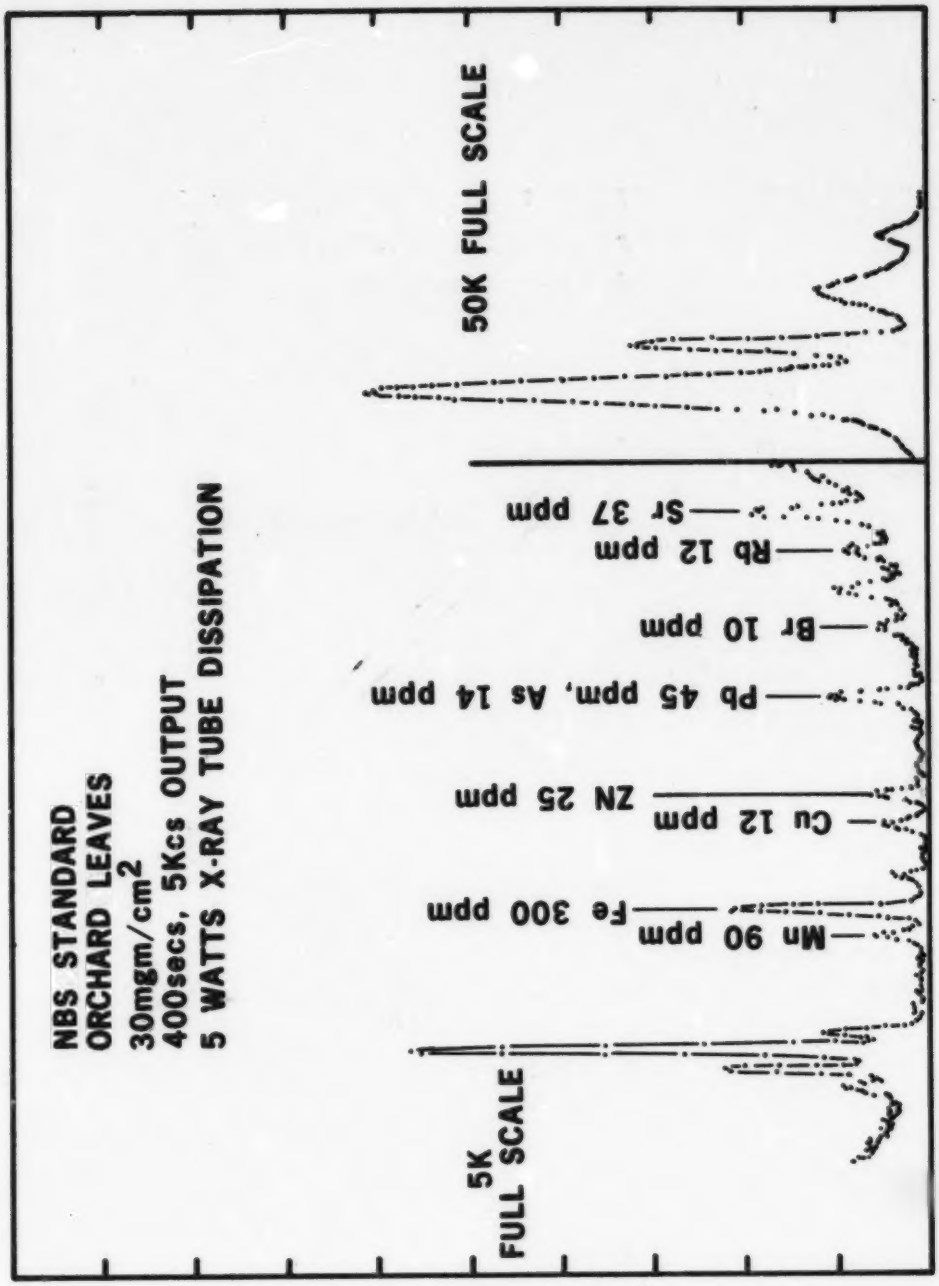

XBL 741-230

Fig. 20

Preceding page blank

APPENDIX A

A. Hardware

The T. I. 960A computer system required as a component in the analysis facility for the 1974 St. Louis RAPS program has been assembled and fully tested. It has been used in studies of the analysis programs and for testing associated hardware as discussed below.

The link between the TI 960A computer and the X-ray system has been changed to eliminate potential and existing noise problems. In place of the multi-wire parallel-driven cable, we now have a 4-coax serial transmission communicator. The communicator consists of two shift registers at the computer and two shift registers at the X-ray machine. The data shifted out of one of the computer shift registers is transmitted via a 120-ohm coaxial cable to the data input lead of one of the X-ray system shift registers. Conversely, data from one of the shift registers at the X-ray machine is transmitted via another 125-ohm coaxial cable to the data input lead of a shift register at the computer. Clock signals, having correct time relationships relative to the data signals are transmitted with each data signal. Thus we have the four coaxial cables linking the two machines.

The reasons for converting to this scheme were two fold.

i) Experience with the existing cable and parallel-transmission scheme demonstrated severe noise problems requiring rather drastic noise-suppression measures.

ii) There was considerable uncertainty regarding the length of the cable in possible future configurations. The production, debugging and

maintenance required to change the four 125-ohm coaxial cables is very small. To change the multi-wire cable is a relatively major job. The characteristic impedence of the cables is 125 ohms and the need for correct relative timing between clock and data signals requires that the cables be of almost the same length. We have successfully tested the system with 30 meter cables separating the computer from the X-ray system. The maximum permissible cable length is a function of cable quality.

B. Software

1. The algorithm used to detect spectrum shifts and correct for them has been thoroughly analyzed. The previous technique involved calculating a residual for the test region at each allowed shift point (up to ± 1 channel in 1/4 channel increments) and selecting the shift value which minimized this residual. This has been changed, with dramatic results, by forcing the centroids of the selected region (one in the reference spectrum and one in the data spectrum) to be equal. This is achieved by using the difference in centroids to approximate the required shift, and then reiterating the process until the centroids converge. To further ensure that the computed shift locates the data spectrum in the center of the "dead-zone" of no-difference in centroid values, the program slides the data spectrum back and forth to determine the boundaries of this dead-zone, and then sets the actual shift value at the center of this dead-zone. The shift increments have also been reduced to 1/16 of a channel.

2. Several convenience features have been added to the program. First, two markers are now available for manipulation, and an option has been added to allow typing out the counts in each channel between the two markers. Second, to allow for expansion of the number of program options available, the operation of the ALT key on the control panel has been changed to make the teletype request an option number, which is then entered from it.

3. Calibration procedures have also been changed. In the CALIBRATE mode, the calibration samples are counted only into buffer 4 (the double precision buffer). When the largest count in the buffer exceeds 960,000 or when the timer terminates the count, the data is divided by a suitable constant to allow it to be stored in a single precision buffer area. The spectrum is then stored on tape for later use.

The new calibration data-entry routines start by the system requesting an option number (Ø-7). Typing a "," makes the routine operate as it did in the original program. Options Ø-7 permit entry into the program at different points, eliminating many redundant requests for information. When the program requests new data it displays the previously stored data.

All spectral calibration data is packed in memory starting at the bottom of the first buffer area. Data relating to the calibration standards inserted by the operator is packed from the top of buffer #5 downwards. Sixteen "descriptor" locations are reserved for each element. If an overlap occurs between incoming spectral data and the "descriptor" area, an error message occurs and some information is not saved.

There is no longer any restriction (except length) on the tag name given to any element. One of the calibration options now allows assigning of an element to an analysis priority group without erasing it from any previous group. One of the regular options destroys all calibration information, producing a virgin program.

4. Error calculations have been improved but further work remains to allow for inter-element effects. Results are now printed out in a fixed sequence going from lighter to heavier elements. Changes have also been made in the output format to minimize typing time.